nature communications

Article

https://doi.org/10.1038/s41467-025-59784-1

Gfi1 controls the formation of effector-like CD8$^+$ T cells during chronic infection and cancer

Received: 16 May 2024

Accepted: 2 May 2025

Published online: 15 May 2025

Check for updates

Oluwagbemiga A. Ojo[1], Hongxing Shen[1], Jennifer T. Ingram[2], James A. Bonner[1], Robert S. Welner[3,4,5], Georges Lacaud[6], Allan J. Zajac[2,4,5] & Lewis Z. Shi[1,2,4,5,7]

During chronic infection and tumor progression, CD8$^+$ T cells lose their effector functions and become exhausted. These exhausted CD8$^+$ T cells are heterogeneous and comprised of progenitors that give rise to effector-like or terminally-exhausted cells. The precise cues and mechanisms directing subset formation are incompletely understood. Here, we show that growth factor independent-1 (Gfi1) is dynamically regulated in exhausted CD8$^+$ T cells. During chronic LCMV Clone 13 infection, a previously under-described Ly108$^+$CX$_3$CR1$^+$ subset expresses low levels of Gfi1 while other established subsets have high expression. Ly108$^+$CX$_3$CR1$^+$ cells possess distinct chromatin profiles and represent a transitory subset that develops to effector-like and terminally-exhausted cells, a process dependent on Gfi1. Similarly, Gfi1 in tumor-infiltrating CD8$^+$ T cells is required for the formation of terminally differentiated cells and endogenous as well as anti-CTLA-induced anti-tumor responses. Taken together, Gfi1 is a key regulator of the subset formation of exhausted CD8$^+$ T cells.

During chronic viral infections (e.g., lymphocytic choriomeningitis virus Clone 13: LCMV Cl-13[1]) and tumor progression, persistent antigen stimulation causes CD8$^+$ T cells to progressively lose their effector functions, a process known as T cell exhaustion[2–6]. Exhausted CD8$^+$ T cells are heterogeneous and maintained by self-renewing TCF1$^+$Ly108$^+$ progenitor cells[4,7–11]. Immune checkpoint blockers (ICB) such as anti-CTLA-4 and anti-PD-1/L1 target progenitor cells and drive their proliferation and differentiation into either Ly108$^-$CX$_3$CR1$^+$ effector-like or Ly108$^-$CX$_3$CR1$^-$ terminally exhausted (Term-Exh) cells[2,4,7,8,11–16]. Formation and maintenance of exhausted effector-like CD8$^+$ T cells is essential for tumor and viral control[4,7,8,15–17]. However, the underlying transcriptional and epigenetic mechanisms remain incompletely understood, delineation of which would help bolster ICB efficacy.

Accumulating evidence indicates that generation of effector-like and Term-Exh subsets involves a substantial chromatin reshaping in progenitor cells[10,18–21], which is under the delicate control of a network of transcription factors (TFs) and signaling pathways. Specifically, TOX is critical for the overall development and maintenance of exhausted CD8$^+$ T cells[22–25], while TCF1 regulates the formation and maintenance of progenitors that is further reinforced by Bach2 and PBAF[9,10,19–21,26]. On the other hand, Batf and Zeb2 mediate the formation of effector-like and Term-Exh cells, but their deletion does not abolish the

[1]Department of Radiation Oncology, Heersink School of Medicine, University of Alabama at Birmingham, Birmingham, AL, USA. [2]Department of Microbiology, Heersink School of Medicine, University of Alabama at Birmingham, Birmingham, AL, USA. [3]Department of Hematology & Oncology, Heersink School of Medicine, University of Alabama at Birmingham, Birmingham, AL, USA. [4]O'Neal Comprehensive Cancer Center, Heersink School of Medicine, University of Alabama at Birmingham, Birmingham, AL, USA. [5]Immunology Institute, Heersink School of Medicine, University of Alabama at Birmingham, Birmingham, AL, USA. [6]Cancer Research UK Manchester Institute, The University of Manchester, Manchester, UK. [7]Department of Pharmacology and Toxicology, Heersink School of Medicine, University of Alabama at Birmingham, Birmingham, AL, USA. e-mail: Lewisshi@uabmc.edu

process[9,12,13,18], suggesting that other TFs also play a role in their formation.

Growth factor-independent 1 (Gfi1) is a transcriptional repressor, consisting of a SNAG domain[27,28] and six zinc-finger motifs, of which the 3–5 motifs are crucial for DNA binding[28]. Gfi1 represses target genes[29–32] through recruitment of histone deacetylases (HDACs), demethylases (KDMs)[33,34], and other chromatin modifying complexes such as CoREST, NuRD, SWI/SNF, and CtBP[35]. Studies from our group and others show that Gfi1 orchestrates the development of thymocytes by repressing Foxo1, Klf2, and Irf4, among others[36,37]. The absence of Gfi1 favors the formation of single positive $CD8^+$ T thymocytes, but its role in mature peripheral $CD8^+$ T cells, especially exhausted $CD8^+$ T cells, has not been studied[36–41]. This can be due in part to the low Gfi1 expression in resting peripheral $CD8^+$ T cells, although Gfi1 is rapidly upregulated upon antigen stimulation[42,43].

Given the persistent antigen stimulation in exhausted T cells[3,44] and the intimate interactions of Gfi1 with chromatin-modifying complexes/epigenetic enzymes, we ask if Gfi1 regulates $CD8^+$ T cell exhaustion. Using Gfi1tdTomato reporter mice, we show that Gfi1 expression is dynamically regulated in exhausted $CD8^+$ T cell subsets during chronic viral infection and tumor progression. In LCMV-specific $CD8^+$ T cells, Gfi1 expression remains low in a newly described $Ly108^+CX_3CR1^+$ subset but high in other subsets. Gfi1 deletion disrupts the repression of epigenetic and transcriptional programs in stem-like progenitor cells as well as the formation of the effector-like and Term-Exh subsets. In tumor-infiltrating T cells (TILs), Gfi1 is highly expressed in a subset of progenitor $CD8^+$ TILs and is required for the accumulation of Tim-3^{hi} terminally differentiated effector TILs. Loss of Gfi1 in T cells dampens effector functions of $CD8^+$ TILs and anti-CTLA-4 efficacy. Overall, we identify Gfi1 as a key regulator of exhausted $CD8^+$ T cell subset diversification during chronic viral infection and cancer progression.

Results

Gfi1 expression in $CD8^+$ T cells is dynamically regulated during chronic viral infection

To monitor Gfi1 expression in $CD8^+$ T cells in response to chronic infections, we utilized the Gfi1 reporter mouse model, wherein endogenous Gfi1 expression is measured by tdTomato[45] (hereafter, Gfi1tdTomato). Gfi1tdTomato mice were infected with LCMV Cl-13, as we previously described[2]. Mice infected with LCMV Armstrong (Arm) were included as controls for acute viral infection. At different times post-infection, splenocytes were harvested and stained with LCMV-D^bGP33 tetramer to determine Gfi1tdTomato expression in LCMV-specific $CD8^+$ T cells. Gfi1tdTomato expression gradually increased in $GP33^+$ $CD8^+$ T cells and reached the peak at the later phase of both acute and chronic viral infections (Day 30, Fig. 1A and Supplementary Fig. S1A). Compared to Arm infection, $CD8^+$ T cells from LCMV Cl-13 infected mice expressed lower levels of Gfi1tdTomato on Day 30 (Supplementary Fig. S1B). To examine the role of Gfi1 in exhausted $CD8^+$ T cells, we focused on its expression in the LCMV Cl-13^+ $CD8^+$ T cell subsets. At the early stage (Days 5–8), Gfi1 expression was negligible in all subsets, defined by Ly108 (a surrogate for the precursor/progenitor marker TCF1[15]) and CX_3CR1 (an effector cell marker[46]) (Supplementary Fig. S1C). On Day 15, when features of exhaustion are being established[9], a considerable proportion of $Ly108^+CX_3CR1^-$ progenitor cells (~ 40–50%) expressed Gfi1 (Supplementary Fig. S1C), while no significant changes between time points were observed in other subsets, indicating an early induction of Gfi1 in exhausted precursor progenitor cells.

On Day 30 post-infection, T cell exhaustion is well established, and the pool of antigen-specific $CD8^+$ T cells is highly heterogeneous[6,9,15]. We thus characterized $GP33^+$ cells by assessing their expression of PD-1, CD44, Ly108, TCF1, Ki67, and CD69, as previously reported[6] (Fig. 1B–D). CD44 expression diminishes as $CD8^+$ T cells become terminally exhausted[2,47,48], dividing $GP33^+$ cells into $CD44^{hi}$ and $CD44^{int}$ fractions. While $CD44^{int}$ cells were homogeneously $Ly108^-TCF1^-$ Term-Exh cells, $CD44^{hi}$ cells can be further divided into $Ly108^+TCF1^+$, $Ly108^+TCF1^-$, and $Ly108^-TCF1^-$ sub-populations (Fig. 1B). Ki67 expression was highest in $Ly108^+TCF1^-$ cells, whereas CD69 expression was highest on $CD44^{int}Ly108^-TCF1^-$ Term-Exh cells, consistent with a previous report[6] (Fig. 1C, D). Ly108 and CX_3CR1 have also been used to define populations of exhausted $CD8^+$ T cells during chronic LCMV Cl-13 infection[15]. We therefore examined their expression on the 4 defined subsets (Fig. 1E). As expected, $CD44^{int}Ly108^-TCF1^-$ Term-Exh cells expressed low levels of CX_3CR1 and Ly108 ($Ly108^-CX_3CR1^-$); progenitor $TCF1^+$ cells were $Ly108^+CX_3CR1^-$, and $CD44^{hi}Ly108^-TCF1^-$ effector-like cells were $Ly108^-CX_3CR1^+$ (Fig. 1E and Supplementary Fig. S1D). Intriguingly, the fourth population of $CD44^{hi}Ly108^+TCF1^-$ cells expressed intermediate CX_3CR1 and Ly108, that is, they were $Ly108^+CX_3CR1^+$ (Fig. 1E and Supplementary Fig. S1D). Further characterizations of these cells revealed that they expressed higher PD-1, 2B4, LAG-3, Tim-3, CD44, Eomes, and TOX but lower T-bet than effector-like cells (Fig. 1F); they also expressed Eomes and Tim-3 at the highest level among all the subsets, suggesting they are different from effector-like cells.

Recent studies have described intermediate or precursor effector subsets based on CXCR6[12] and KLRG1[13,14] expression. We therefore characterized their expression on the 4 exhausted subsets. While CXCR6 was not observed on progenitor or $Ly108^+CX_3CR1^+$ cells (Fig. 1G), KLRG1 was expressed on both $Ly108^+CX_3CR1^+$ and effector-like cells (Supplementary Fig. S1E). Functionally, $Ly108^+CX_3CR1^+$ cells produced more IFN-γ than other exhausted subsets, but this was negligible compared to $CD8^+$ T cells from LCMV Arm infection (Supplementary Fig. S1F, Top). On the other hand, effector-like cells produced more perforin than $Ly108^+CX_3CR1^+$ cells (Supplementary Fig. S1F, Bottom). Contrasting to $CD8^+$ T cells from Arm infection, these LCMV Cl-13 exhausted cells did not produce substantial amounts of TNF. We then analyzed Gfi1tdTomato expression in these exhausted subsets. Gfi1tdTomato was highly expressed in the progenitor, effector-like, and Term-Exh subsets but lowly expressed in $Ly108^+CX_3CR1^+$ cells (Fig. 1H). In sum, using Ly108 and CX_3CR1, we can define 4 exhausted subsets on Day 30 post LCMV Cl-13 infection: $Ly108^+CX_3CR1^-$ progenitors, $Ly108^+CX_3CR1^+$ cells, $Ly108^-CX_3CR1^+$ effector-like cells, and $Ly108^-CX_3CR1^-$ terminally exhausted cells (Term-Exh), which differentially express Gfi1.

$Ly108^+CX_3CR1^+$ cells possess unique chromatin accessibility and transcriptional features, some of which are shared with effector-like cells

Our above characterizations and differential Gfi1 expression of $Ly108^+CX_3CR1^+$ cells suggest they are a distinct exhausted subset. Considering the essential role of epigenetic and transcriptomic imprinting of exhausted $CD8^+$ T cells[18,20,21,26,49–51], we hypothesized that $Ly108^+CX_3CR1^+$ cells would possess distinct chromatin accessibility and transcriptomic profiles. To examine this, sorted progenitors, $Ly108^+CX_3CR1^+$, effector-like, and Term-Exh $GP33^+$ $CD8^+$ cells from WT non-Gfi1tdTomato reporter mice were subject to Assay for Transposase-Accessible Chromatin with sequencing (ATAC-seq). Since progenitors are the source of the other subsets during chronic viral infection[6,9], we focused on statistically significant chromatin changes in $Ly108^+CX_3CR1^+$ versus progenitor cells, using a ≥ 1.2 log2 fold change as the cutoff. Overall, $Ly108^+CX_3CR1^+$ cells had 3218 differentially accessible chromatin regions (DACR) with increased accessibility and 633 DACRs with decreased accessibility (Fig. 2A). Most of these DACRs were localized at enhancers (distal intergenic and intronic regions) in accordance with the concept that these regions determine cellular identity[52] (Fig. 2B). We then visualized these DACRs in effector-like and Term-Exh subsets to evaluate their accessibility. As shown in Fig. 2C, $Ly108^+CX_3CR1^+$ and effector-like cells shared similar accessibility profiles in some regions (Cluster 1 and Supplementary Data File 1; e.g., *Havcr2* encoding Tim-3). We also identified regions (Clusters 3 and 4;

https://doi.org/10.1038/s41467-025-59784-1

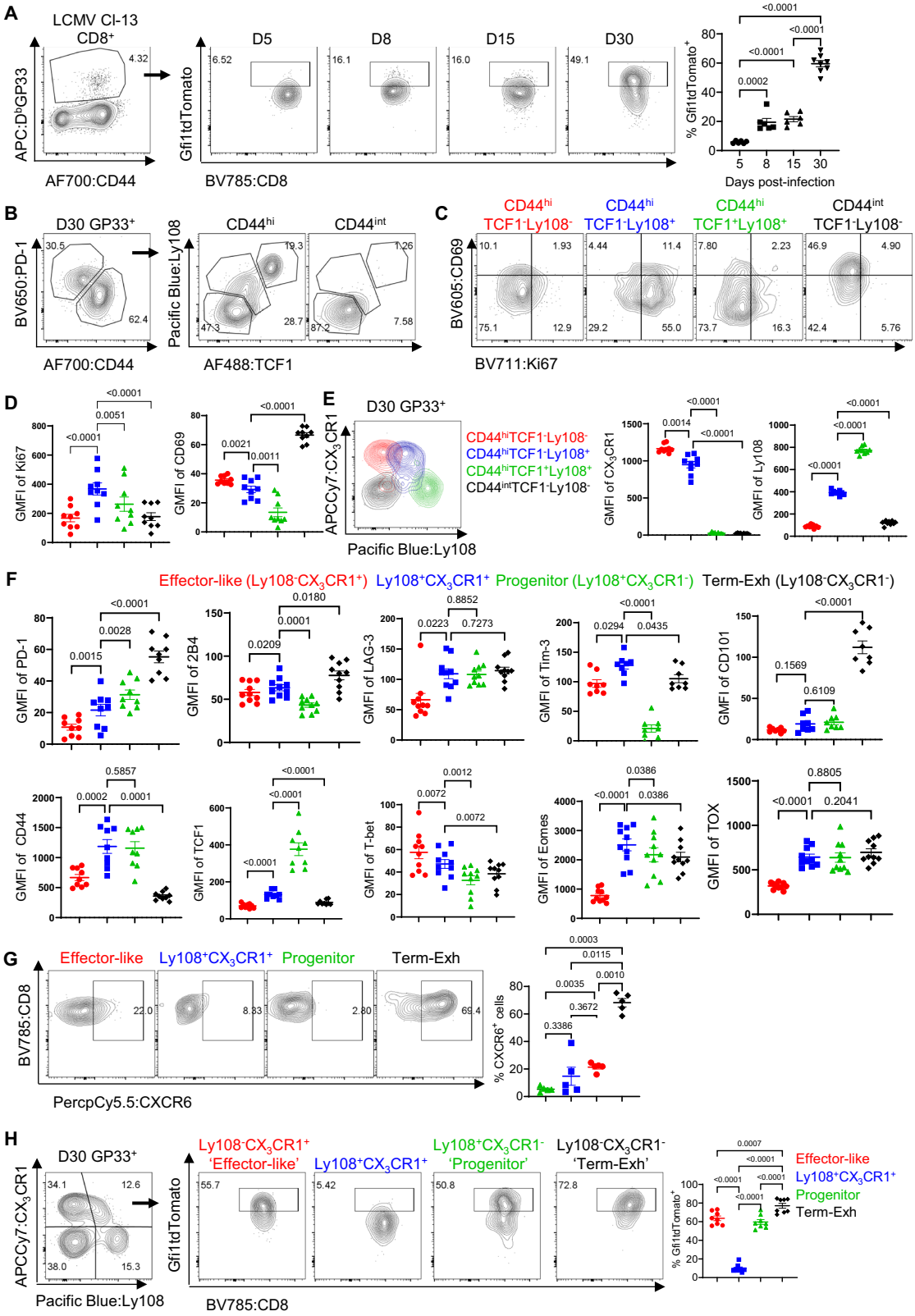

e.g., *Batf3*) in which Ly108$^+$CX$_3$CR1$^+$ cells had the greatest increase in accessibility compared to other subsets.

Next, we performed direct pairwise comparisons between Ly108$^+$CX$_3$CR1$^+$ or progenitor cells versus other subsets (Fig. 2A and Supplementary Data File 1). To our surprise, we detected only 30 more but no less accessible DACRs in Ly108$^+$CX$_3$CR1$^+$ compared to effector-like cells. This limited number of DACRs could be due to similar chromatin accessibility profiles between them or a lack of statistical power to detect such differences. In contrast, there were 9368 and 2682 DACRs between effector-like and progenitor or Term-Exh cells, respectively, indicating our data were sufficiently powered (Fig. 2A). Next, we determined the shared or unique DACRs between Ly108$^+$CX$_3$CR1$^+$ and effector-like subsets when compared to progenitor cells (Fig. 2D). Strikingly, 77% of identified DACRs in

Fig. 1 | Gfi1 is dynamically regulated in exhausted CD8$^+$ T cell subsets during chronic viral infection. A Gfi1tdTomato reporter mice were infected with LCMV Cl-13, followed by the assessment of Gfi1tdTomato expression on Days 5 ($n = 6$), 8 ($n = 6$), 15 ($n = 6$) and 30 ($n = 8$) post-infection. **B**–**E** Identification of Day 30 exhausted CD8$^+$ T cell subsets based on CD44, PD-1, TCF1, Ly108 (B), Ki67, and CD69 expression (**C**). **D** Quantification of Ki67 and CD69 expressions as in (**C**) ($n = 9$). E. Expression and quantification of Ly108 and CX_3CR1 on the 4 exhausted subsets ($n = 9$). **F** GMFIs of PD-1, 2B4, LAG-3, Tim-3, CX_3CR1, CD44, TCF1, T-bet, Eomes, and TOX in the 4 exhausted subsets (progenitor, Ly108$^+$CX$_3$CR1$^+$, effector-like, and Term-Exh) ($n = 9$–10). **G** Expression and quantification of CXCR6 in the 4 exhausted subsets ($n = 5$). **H** Gfi1tdTomato expression on the 4 exhausted CD8$^+$ T cell subsets ($n = 8$). Data were pooled from 2 independent experiments and depicted with mean ± s.e.m. Data in A were analyzed by one-way ANOVA; data in (**D**–**H**) were analyzed by repeated one-way ANOVA. Holm-Sidak's post hoc test was used for all analysis. Source data are provided as a Source Data file.

Ly108$^+$CX$_3$CR1$^+$ versus progenitors were also identified in effector-like cells (2972 out of 3851 DACRs), but 68% of identified DACRs in effector-like versus progenitors were unique to effector-like cells and not shared with Ly108$^+$CX$_3$CR1$^+$ cells (6396 out of 9368 DACRs) (Fig. 2D). Visualization of the inferred 6396 DACRs 'unique' to effector-like cells revealed that Ly108$^+$CX$_3$CR1$^+$ cells had an intermediate chromatin accessibility profile in these regions between progenitor and effector-like cells (Fig. 2D and Supplementary Data File 1, inferred DPvsEff). Specifically, 3465 DACRs were less accessible (e.g., *Brwd1*, *Hrh4, Wnt3, Smarca2*, and *Setd2*) whilst the other 2931 DACRs were more accessible (e.g., *Ccl3, Zeb2, Klrb1c, Glp1r, and Jun*) in effector-like cells than progenitors cells. More accessible 2931 DACRs were linked to pathways involving GTPase activity and downstream NFAT and AP1 activity important for T cell activation[53] (Supplementary Fig. S2B), while less accessible 3465 DACRs were associated with Wnt signaling, etc. known to inhibit effector differentiation[54]. Finally, we identified 6672 less (e.g., *Klrg1, CD86, Kat7*) and 1549 more (e.g., *Sirt4, Hdac4, and Glp1r*) accessible DACRs in Term-Exh than Ly108$^+$CX$_3$CR1$^+$ cells (Fig. 2E). Several of the identified DACRs between Ly108$^+$CX$_3$CR1$^+$ and progenitors, effector-like or Term-Exh cells included loci previously associated with T cell exhaustion and/or differentiation such as *Zeb2*[12], *Batf3*[55], *Hif1a*[56], *Irf4*[57], *Irf5*[58], *Batf*[9,18,49], *Glp1r*[59,60], and *Runx3*[49,61–64] as well as those with previously unreported roles in T cell exhaustion such as *Mef2c*. Genomic tracks for the *Mef2c, Zeb2* and *Batf3*, and *Glp1r* loci were shown in Fig. 2F and Supplementary Fig. S2A. Overall, these results suggest that Ly108$^+$CX$_3$CR1$^+$ and effector-like cells share some chromatin accessibility profiles, but there are numerous and subtle differences between them. Furthermore, Ly108$^+$CX$_3$CR1$^+$ cells appear to be more distinctively different from progenitors and Term-Exh cells.

We then predicted the transcription factors (TFs) interacting with DACRs in Ly108$^+$CX$_3$CR1$^+$, effector-like, and Term-Exh cells by performing de novo motif analysis using HOMER[65]. As expected, motifs for TFs with previously reported roles in CD8$^+$ T cell effector functions, such as Batf, AP-1/NFAT and IRF family proteins[18,49,50,57,66–70] were enriched in DACRs identified in Ly108$^+$CX$_3$CR1$^+$ and effector-like cells (Fig. 2G and Supplementary Fig. S2C). Interestingly, we also observed Gfi1 DNA binding motif (5'-AAATC-3')[28,71,72] in DACRs identified in Ly108$^+$CX$_3$CR1$^+$ cells versus progenitor, effector-like, or Term-Exh cells (Supplementary Fig. S2D); regions within the Gfi1 locus were differentially accessible among the subsets (Supplementary Fig. S2A, Bottom), although the role of Gfi1 in T cell exhaustion has been unreported.

To understand the transcriptomic profiles of the 4 subsets, we performed RNA-seq. Pairwise comparisons unveiled 1279 differentially expressed genes (DEGs) between Ly108$^+$CX$_3$CR1$^+$ and progenitor cells, 499 DEGs between Ly108$^+$CX$_3$CR1$^+$ and effector-like cells, and 1392 DEGs between Ly108$^+$CX$_3$CR1$^+$ and Term-Exh cells (Supplementary Data File 2), further supporting Ly108$^+$CX$_3$CR1$^+$ are a distinct subset. For illustrative purposes, select transcripts of transcription factors (Fig. 2H) and effector molecules (Fig. S2E) among DEGs were shown. TFs (e.g., *Irf8, Irf5, Foxm1*, and *Hmgb3*) and molecules associated with cell proliferation, such as *Mybl2,* were significantly increased in Ly108$^+$CX$_3$CR1$^+$ cells compared to the other subsets. Interestingly, *Zeb2, Pou2f1, Spi1, E2F2/7/8 proteins, Hmgb2*, and *Hmgn5* were significantly elevated in Ly108$^+$CX$_3$CR1$^+$ and effector-like cells compared to progenitors and Term-Exh cells, suggesting these TFs may co-regulate effector-like and Ly108$^+$CX$_3$CR1$^+$ cells. Among DEGs between effector-like and Ly108$^+$CX$_3$CR1$^+$cells, higher expression of *Prf1* (encodes Perforin*)*, *Ccl3*, *Id2,* and *Glp1r* but lower expression of *Myb, Mef2c, Hmgn3, Pou2af1*, and *Spib* were found in Ly108$^+$CX$_3$CR1$^+$cells than in effector-like cells. Surprisingly, normalized Gfi1 mRNA values from the sequencing experiment were comparable between Ly108$^+$CX$_3$CR1$^+$ and progenitor cells, which were lower than Term-Exh and effector-like cells (Supplementary Fig. S2F). We speculate the relatively low Gfi1 mRNA values in progenitors may be due to a high fraction of Gfi1^{lo} cells in this subset.

CD8$^+$ T cell intrinsic Gfi1 is required for the formation of effector-like and Term-Exh cells

The dynamic regulation of Gfi1 reporter expression, the enrichment of Gfi1 motif in DACRs, and the unreported role of Gfi1 in T cell exhaustion prompted us to examine whether and how Gfi1 modulates exhausted CD8$^+$ T cells. To this end, we generated mice with specific Gfi1 deletion in T cells by crossing floxed Gfi1 mice with CD4-Cre transgenic mice (hereafter, Gfi1^{cKO})[36,38,41]. As we previously described[36,41], the zinc finger region 3-5 of Gfi1, essential for DNA binding and transcriptional activity[28] are deleted in Gfi1^{cKO} T cells. Gfi1$^{fl/fl}$CD4-Cre$^{-/-}$ littermates (WT) and Gfi1^{cKO} mice were infected with LCMV Cl-13. On Days 15-16 and 30-45 post-infection, GP33$^+$ T cells from the spleen were analyzed. Although the frequencies of total GP33$^+$ CD8$^+$ T cells were similar on Day 15, total cell numbers were lower in Gfi1^{cKO} mice at this time point ($p = 0.0549$, Supplementary Fig. S3A). On Day 30, when the CD8$^+$ T cell responses contracted, both the frequency and cell number of total GP33$^+$ CD8$^+$ cells were comparable between Gfi1^{cKO} and WT mice. We then evaluated the impact of Gfi1 deletion on the subset diversification of exhausted GP33$^+$ CD8$^+$ T cells, categorized by Ly108 and CX_3CR1. As shown in Fig. 3A, B, Gfi1^{cKO} cells failed to generate effector-like and Term-Exh subsets, but the progenitor and Ly108$^+$CX$_3$CR1$^+$ subsets appeared unaltered. In support of this, KLRG1, a killer-type lectin that has been linked to the effector-like subset[13,14], was not expressed by Gfi1^{cKO} cells (Supplementary Fig. S3B). Failed formation of effector-like and Term-Exh cells was also observed in the GP33$^+$ CD8$^+$ T cells from the liver (Supplementary Fig. S3C, D), with the cell number of total GP33$^+$ CD8$^+$ T cells significantly reduced in Gfi1^{cKO} mice and their frequencies being comparable to WT mice (Supplementary Fig. S3D).

To further demonstrate the failed formation of effector-like and Term-Exh subsets by Gfi1^{cKO} cells, we assessed the expression of CD44, PD-1, Ly108, and TCF1 (Supplementary Fig. S3E). We did not detect CD44^{int} or Ly108$^-$ cells in the absence of Gfi1, further supporting the lack of Term-Exh and/or effector-like cells. We also considered whether this phenotype was due to increased cell death in the absence of Gfi1. However, pan-caspase expression was similar between WT and Gfi1^{cKO} progenitors and Ly108$^+$CX$_3$CR1$^+$ cells (Supplementary Fig. S3F), ruling out that possibility. We did observe a significant decrease in Ki67 expression between WT and Gfi1^{cKO} Ly108$^+$CX$_3$CR1$^+$ cells, although no overt difference was observed in progenitor cells (Supplementary Fig. S3G).

We next quantified the expression of inhibitory receptors and TFs associated with T cell exhaustion in WT and Gfi1^{cKO} subsets. TOX, LAG-

https://doi.org/10.1038/s41467-025-59784-1

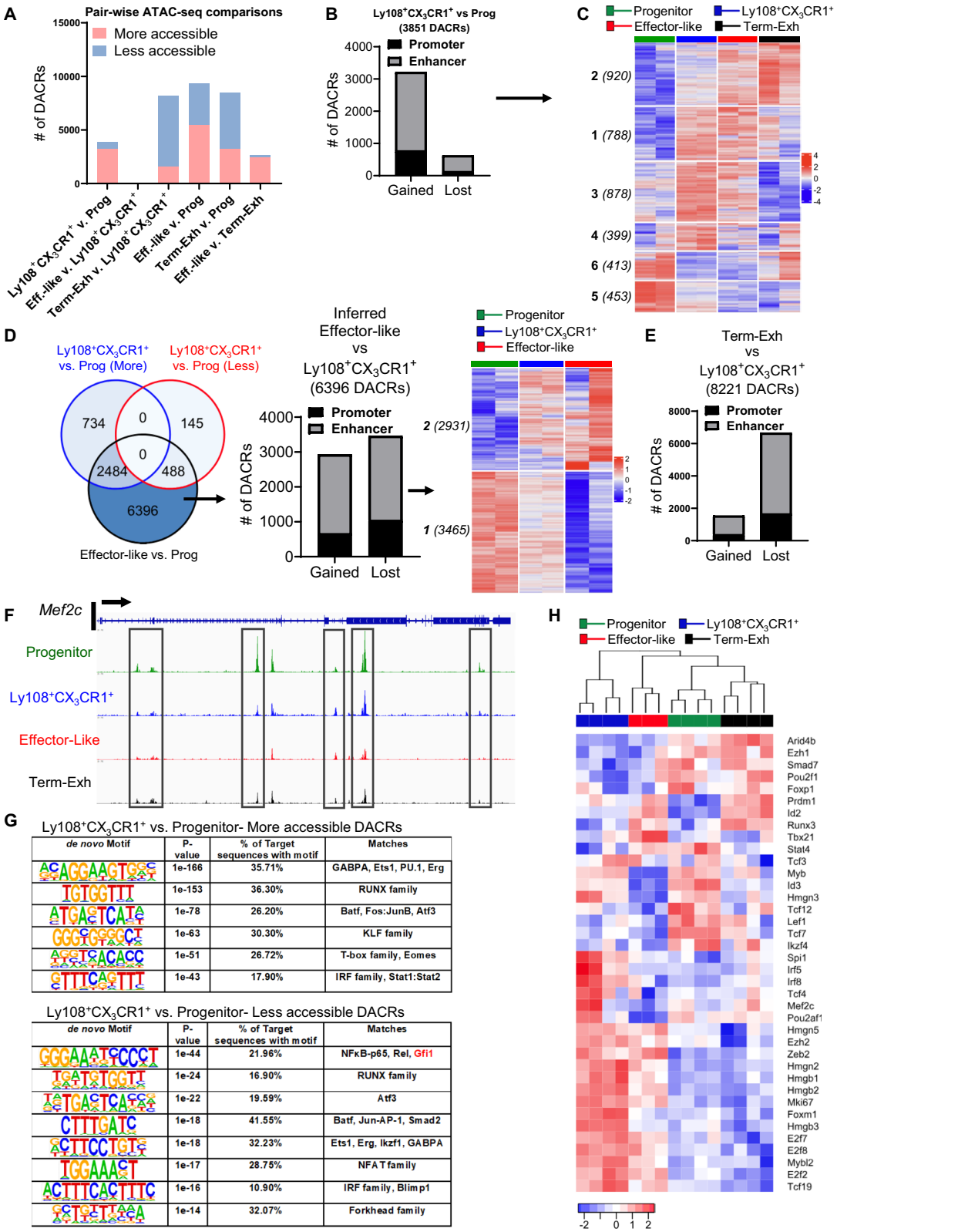

3, and Tim-3 were significantly upregulated in both Gfi1^{cKO} subsets compared to WT cells (Supplementary Fig. S3H). Interestingly, we observed increased Eomes and decreased TCF1 expression only within Gfi1^{cKO} progenitors, while PD-1 was significantly increased in Gfi1^{cKO} Ly108^{+}CX$_3$CR1^{+} cells compared to their WT counterparts (Supplementary Fig. S3H). Functionally, granzyme B (GzmB) expression was lower in Gfi1^{cKO} Ly108^{+}CX$_3$CR1^{+} than WT cells (Supplementary Fig. S3I, right), although no overt differences in IFN-γ and TNF production were observed between WT and Gfi1^{cKO} cells (Supplementary Fig. S3I, left). In keeping with the absence of effector-like cells[15] and reduced cytolytic capabilities of Gfi1^{cKO} Ly108^{+}CX$_3$CR1^{+} cells (i.e., reduced GzmB), Gfi1^{cKO} mice had elevated viral titers at later time points (Days 30 and beyond, Supplementary Fig. S3J).

CD4^{+} T cell deficiency ablates the formation of exhausted effector-like CD8^{+} T cells[15,73]. Since our model deletes Gfi1 in both CD8^{+} and CD4^{+} T cells, we wanted to rule out potential confounding effects from

Fig. 2 | Ly108$^+$CX$_3$CR1$^+$ cells possess unique chromatin accessibility and transcriptional features, some of which are shared with effector-like cells. Day 30 exhausted GP33$^+$ CD8$^+$ T cell subsets were sorted based on Ly108 and CX$_3$CR1 expression for ATAC-Seq (**A**–**G**) and RNA-Seq (**H**). **A** Statistically significant and differentially accessible chromatin regions (DACRs) with >1.2 log2 fold change from pairwise comparisons were shown. Prog = Progenitor, Eff-like = Effector-like, and Term-Exh = Terminally-exhausted. **B** Promoter and Enhancer distribution of more and less accessible DACRs in the Ly108$^+$CX$_3$CR1$^+$ cells versus progenitors. **C** Accessibility profiles of DACRS from (**B**) were visualized in effector-like and Term-Exh cells. **D** Venn diagram depicting the intersection of DACRs in Ly108$^+$CX$_3$CR1$^+$ cells versus progenitors with those in effector-like cells versus progenitors (Left), with the bar graph showing the unique DACRs in effector-like cells (Middle), and heatmap visualization of these regions in progenitors, Ly108$^+$CX$_3$CR1$^+$, and effector-like cells (Right). **E** Bar graph depicting distribution of DACRs in Term-Exh versus Ly108$^+$CX$_3$CR1$^+$ cells. **F** Genomic track of accessibility at the *Mef2c* locus in the 4 exhausted subsets. **G** De novo HOMER motif analysis of DACRs from Ly108$^+$CX$_3$CR1$^+$ versus progenitor cells. **H** Heatmap visualization of select transcription factors among the 4 exhausted subsets. ATAC- and RNA-seq data were from 2 and 3-4 independent replicates, respectively. Each replicate was a pooled sample of 3-5 mice.

Gfi1^{cKO} CD4$^+$ T cells by depleting CD4$^+$ T cells in vivo. As previously reported[15,73], CD4 depletion promoted exhaustion in WT GP33$^+$ CD8$^+$ T cells (Fig. 3C versus 3A) and resulted in reduced effector-like cells. Like un-manipulated mice, no significant differences in total GP33$^+$ frequencies and numbers were observed in CD4-depleted Gfi1^{cKO} mice on Days 15 and 30 (Supplementary Fig. S3K). Interestingly, the numbers of progenitors and Ly108$^+$CX$_3$CR1$^+$ cells were comparable between WT and Gfi1^{cKO} mice with CD4$^+$ T cell depletion, contrasting their increases in un-manipulated Gfi1^{cKO} mice (Fig. 3B, D), suggesting a role of CD4$^+$ T cells in maintaining their overall numbers. Nevertheless, we still observed significantly impaired formation of effector-like and Term-Exh cells in CD4-depleted Gfi1^{cKO} mice (Fig. 3C, D). To firmly establish this is a CD8$^+$ T cell intrinsic effect, we employed the bone marrow chimeric mice (BM) reconstituted with wild-type or Gfi1^{cKO} BM cells. Following reconstitution, these mice were infected with LCMV Cl-13. GP33$^+$ CD8$^+$ splenocytes were analyzed on Day 30. As shown in Fig. 3E, WT CD45.1$^+$ and CD45.2$^+$ GP33$^+$ cells successfully generated progenitor, Ly108$^+$CX$_3$CR1$^+$, effector-like, and Term-Exh cells, but CD45.2$^+$ Gfi1^{cKO} GP33$^+$ cells were still unable to form effector-like and Term-Exh cells even in the presence of wild-type CD4$^+$ T cells. Again, there were no significant differences in total GP33$^+$ frequencies and cell counts in the spleens of BM chimeras (Supplementary Fig. S3L). These data highlight a CD8$^+$ T cell intrinsic role for Gfi1 in the formation of effector-like and Term-Exh subsets.

Transitional Ly108$^+$CX$_3$CR1$^+$ cells develop into effector-like and Term-Exh subsets

Considering the shared chromatin accessibility and transcriptomic landscape between Ly108$^+$CX$_3$CR1$^+$ and effector-like cells, as well as the inability of Gfi1^{cKO} CD8$^+$ T cells to form effector-like and Term-Exh subsets, we next assessed their developmental potential. To this end, we sorted progenitor, Ly108$^+$CX$_3$CR1$^+$, effector-like, and Term-Exh subsets from Day 30 LCMV Cl-13 infected Gfi1tdTomato mice and adoptively transferred them into naïve CD45.1$^+$ recipients, followed by LCMV Cl-13 on the next day. The progenies of the transferred cells (CD45.2$^+$) were analyzed on Day 8 post-secondary infection. As previously reported, effector-like and Term-Exh cells largely retained their phenotype[15], and progenitors were capable of re-generating all the subsets (Fig. 3F and Supplementary Fig. S4A). However, transferred Ly108$^+$CX$_3$CR1$^+$ cells were only able to form effector-like and Term-Exh but not progenitors (Fig. 3F). Noteworthily, some Ly108$^+$CX$_3$CR1$^+$ cells retained their identify on Day 8 after transfer, indicating some degree of stability. Transferred progenitors were recovered at the highest frequencies and numbers, although this did not reach statistical significance compared to other transferred subsets (Fig. 3F and Supplementary Fig. S4A).

The adoptive transfer studies suggest that differentiation of Ly108$^+$CX$_3$CR1$^+$ cells (Gfi1tdTomato^{lo}) to effector-like and Term-Exh cells (Gfi1tdTomato^{hi}) is coupled with an increase of Gfi1tdTomato expression (Supplementary Fig. S4B). Considering that Gfi1tdtomato^{lo} cells persisted in the progenitor, effector-like, and Term-Exh subsets (Fig. 1H), we characterized the expression of some key TFs, inhibitory receptors, and proteins within Gfi1tdTomato^{hi} and Gfi1tdTomato^{lo} fractions to shed light on their potential interactions with Gfi1 (Supplementary Fig. S4C, D). Eomes, TOX, and Tim-3 expression were significantly elevated in Gfi1tdtomato^{lo} compared to Gfi1tdTomato^{hi} fractions in all 3 subsets (Supplementary Fig. S4C, D). The reciprocally lower PD-1 and higher T-bet in Gfi1tdTomato^{lo} than Gfi1tdTomato^{lo} Term-Exh supported a previously-reported strong repression of the *Pdcd1* loci by T-bet[74], but this was restricted to that subset, as there were no significant differences of PD-1 and T-bet expression between Gfi1tdTomato^{hi} and Gfi1tdTomato^{lo} progenitors and effector-like cells (Supplementary Fig. S4C). Finally, CX$_3$CR1 expression was higher in Gfi1tdTomato^{lo} progenitor and Term-Exh subsets but lower in Gfi1tdTomato^{lo} effector-like cells compared to their Gfi1tdTomato^{hi} counterparts (Supplementary Fig. S4D). These data were consistent with the greater CX$_3$CR1 expression in Ly108$^+$CX$_3$CR1$^+$ and effector-like cells (Fig. 1E), in line with their developmental potentials. Taken together, these data unveil a possible repression of Eomes, TOX, and Tim-3 by Gfi1 in exhausted CD8$^+$ T cell subsets.

TCF1 maintains progenitors and is downregulated as these cells differentiate[4,9,10]. Given the downregulated TCF1 and Ly108 (surrogate marker for TCF1) in Gfi1tdTomato^{lo} progenitor cells (Supplementary Fig. S4C, D), we asked if the Gfi1tdTomato^{lo} progenitor fraction was more poised to differentiate into other subsets than the Gfi1tdTomato^{hi} progenitor fraction. To address this, Gfi1tdTomato^{lo} and Gfi1tdTomato^{hi} progenitor cells sorted from Day 30 LCMV Cl-13 infected Gfi1tdTomato mice were transferred into naïve CD45.1$^+$ mice and subsequently infected with LCMV Cl-13 one day later. Eight days post-infection, both progenitor fractions (CD45.2$^+$) regenerated all other subsets, although more cells were recovered from transferred Gfi1tdTomato^{hi} progenitors (Supplementary Fig. S4E). Interestingly, Gfi1tdtomato expression was increased in recovered cells from transferred Gfi1tdTomato^{lo} progenitors (Supplementary Fig. S4E), indicating a reversible conversion between Gfi1tdTomato^{lo} and Gfi1tdTomato^{hi} progenitors.

Gfi1 modulates the chromatin accessibility and transcriptomic programs associated with the formation of exhausted effector-like and Term-Exh CD8$^+$ T cells

Epigenetic changes underpin the formation of T cell subsets during chronic viral infection[14,18,20–22,26,51,75]. Given Gfi1's reported functions in chromatin modifying complexes in other cellular contexts[33–35], we posited that Gfi1 would impact the chromatin accessibility associated with the differentiation of exhausted CD8$^+$ T cell subsets. To test this idea, sorted splenic GP33$^+$ progenitor and Ly108$^+$CX$_3$CR1$^+$ cells from Day 30 LCMV Cl-13 infected Gfi1^{cKO} mice, together with WT subsets, were subject to ATAC-seq and RNA-seq. We identified 693 (647 more and 46 less accessible) and 2471 (1109 more and 1362 less accessible) DACRs between Gfi1^{cKO} and WT progenitors and Ly108$^+$CX$_3$CR1$^+$ cells, respectively (Fig. 4A, Supplementary Fig. S5A, B and Supplementary Data File 3).

Given that Ly108$^+$CX$_3$CR1$^+$ cells can be formed with or without Gfi1, we asked whether the chromatin accessibility changes observed in WT cells during the transition from progenitors to Ly108$^+$CX$_3$CR1$^+$ cells would also occur in Gfi1^{cKO} cells. Remarkably, only 30 more and

https://doi.org/10.1038/s41467-025-59784-1

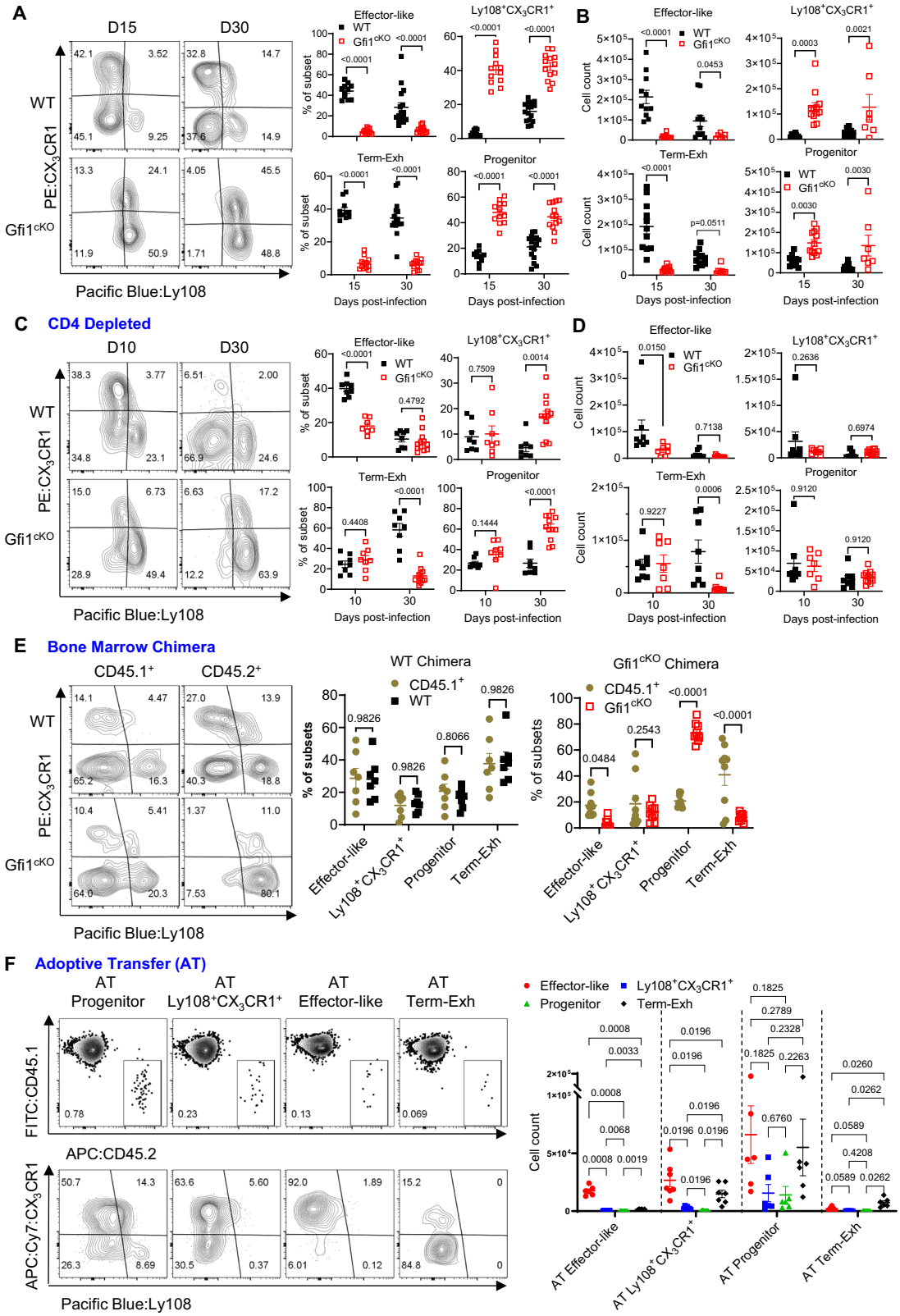

164 less accessible DACRs were identified in Gfi1^{cKO} Ly108^{+}CX$_3$CR1^{+} cells versus progenitors, in contrast to 3218 more and 633 less accessible DACRs in WT cells (Fig. 4B, Supplementary Fig. S5C and Supplementary Data File 3). For illustrative purposes, we visualized all the identified DACRs in both Gfi1^{cKO} subsets compared to their WT counterparts to understand how loss of Gfi1 impacted chromatin accessibility and prevented the formation of effector-like cells (Fig. 4C). Some regions (cluster 4), including *Mef2c* (Fig. 4D, denoted with a red star), *Foxp1* (Fig. 4D, Bottom), *Irf4, and Nt5e* (encodes *CD73* and is repressed by Gfi1[76]), failed to lose accessibility in Gfi1^{cKO} Ly108^{+}CX$_3$CR1^{+} cells, and rather increase accessibility compared to WT cells. Of note, these regions became less accessible in WT effector-like than in progenitors or Ly108^{+}CX$_3$CR1^{+} cells (Fig. 4D Top and Supplementary Data File 3), indicating their lost accessibility is needed for the formation of

Fig. 3 | CD8⁺ T cell intrinsic Gfi1 is required for the formation of effector and Term-Exh subsets. A, **B** GP33⁺ responses were evaluated in WT and Gfi1^{cKO} mice on Days 15 and 30 post LCMV Cl-13 infection. Frequencies (**A**) and cell numbers (**B**) of subsets (in **A**, $n = 11$ and 16 for WT mice, 12 and 13 for Gfi1^{cKO} mice on Day 15 and 30, respectively. For (**B**), $n = 11$ for WT mice at both time points, and $n = 12$ and 7 for Gfi1^{cKO} mice on Day 15 and 30, respectively). **C**, **D**. Frequencies (**C**) and cell numbers (**D**) of GP33 + subsets in CD4-depleted WT ($n = 8$ for both time points) and Gfi1^{cKO} mice ($n = 7$ and 12, respectively, for Day 15 and 30). **E** CD45.1⁺ mice reconstituted with WT ($n = 7$) or Gfi1^{cKO} ($n = 9$) CD45.2⁺ BM cells (chimeric mice) were infected with LCMV Cl-13. GP33⁺ CD8⁺ T cell responses in CD45.1⁺ and CD45.2⁺ compartments were analyzed on Day 30 post-infection. **F** Sorted exhausted subsets (Progenitors: $n = 6$; Ly108⁺CX$_3$CR1⁺: $n = 7$; effector-like: $n = 6$; Term-Exh: $n = 6$) from Day 30 LCMV Cl-123-infected Gfi1tdTomato reporter mice were adoptively transferred into naïve CD45.1⁺ recipients, followed by LCMV Cl-13 infection on the next day. Progenies of adoptively transferred cells were characterized for their expression of Ly108 and CX$_3$CR1 on Day 8 post-infection. Cell counts of subsets were shown by the scatter dot plot. Data (mean ± s.e.m) were pooled from 2-4 independent experiments and analyzed by two-way ANOVA with Holm-Sidak's post-hoc test. Source data are provided as a Source Data file.

effector-like cells. On the contrary, other regions (cluster 2), including *Dnmt3a*, *Akt2*, *Runx1*, and *Runx3*, failed to gain accessibility in Gfi1^{cKO} Ly108⁺CX$_3$CR1⁺ cells versus progenitors, which was evident in WT Ly108⁺CX$_3$CR1⁺ cells. Finally, we identified regions such as in *Havcr2* (encodes Tim-3, Supplementary Fig. S5D, Middle), *Mef2c*, and *Ezh1* (Supplementary Fig. S5D, Top) with significantly increased accessibility in Gfi1^{cKO} progenitors and Ly108⁺CX$_3$CR1⁺ cells compared to their WT counterparts. Taken together, the dearth of DACRs in Gfi1^{cKO} Ly108⁺CX$_3$CR1⁺ cells versus progenitors cells can be explained by the premature increase in accessibility in cluster 3 within progenitor cells and the failure of Ly108⁺CX$_3$CR1⁺ to lose accessibility in cluster 4 in the absence of Gfi1.

De novo motif analysis on the DACRs between the WT and Gfi1^{cKO} progenitors and Ly108⁺CX$_3$CR1⁺ cells identified enrichment of TFs such as Batf[18,49], CTCF[77], and NFAT[78] (Fig. 4E and Supplementary Fig. S5E). Consistent with the auto-repression of the *Gfi1* locus by Gfi1 itself[32,43], its motifs were enriched in accessible regions in both Gfi1^{cKO} progenitors and Ly108⁺CX$_3$CR1⁺ cells compared to WT cells (Fig. S5D, E). We detected Gfi1 binding motifs at *Havcr2 regions* with increased chromatin accessibility in Gfi1^{cKO} compared to WT cells (Supplementary Data File 3), which was consistent with the increased Tim-3 expression in Gfi1tdTomato^{lo} subsets (Supplementary Fig. S4F) and in Gfi1^{cKO} cells (Supplementary Fig. S3H). Notably, the chromatin dysregulation in the absence of Gfi1 was observed only in exhausted antigen-specific cells but not naïve CD8⁺ T cells, in line with negligible Gfi1 protein expression in naive cells (Supplementary Fig. S5F).

RNA-seq analyses of Gfi1^{cKO} subsets and their WT counterparts also revealed dysregulated transcriptomes, which were congruent in part with our ATAC-seq analysis. As detailed in Supplementary Data File 4, we detected 55 DEGs between WT and Gfi1^{cKO} progenitors, 488 DEGs between WT and Gfi1^{cKO} Ly108⁺CX$_3$CR1⁺ cells, and 515 DEGs between Gfi1^{cKO} Ly108⁺CX$_3$CR1⁺ and progenitor cells. For illustrative purposes, select transcripts for TFs and activation markers were visualized to highlight the impact of Gfi1 on transcriptomes (Fig. 4F and Supplementary Fig. S5G). Understandably, some transcriptomic programs such as upregulation of *Irf8, Spi1*, and *Zeb2*, and *Hmgn2*, and downregulation of *TCF7, Id3,* and *Satb1* were maintained in Gfi1^{cKO} Ly108⁺CX$_3$CR1⁺ cells compared to progenitors (Fig. 4F and Supplementary Data File 4). On the other hand, several repression programs in Ly108⁺CX$_3$CR1⁺ cells were dysregulated in the absence of Gfi1. Gfi1^{cKO} Ly108⁺CX$_3$CR1⁺ cells aberrantly exhibited upregulated *Batf, Lef1, Ikzf2, Hif1a, TOX, Stat4, Irf2, Runx2, and Runx3* but downregulated *Spib, Bmyc, Myc, Pou2af1, Klrg1, and Ifngr2* compared to WT Ly108⁺CX$_3$CR1⁺ cells (Fig. 4F and Supplementary Data File 4). Transcripts for *Hrh4, Kit, Glp1r, Havcr2, and LAG-3* were significantly increased in both Gfi1^{cKO} subsets compared to WT subsets (Supplementary Fig. S5G). Because CD101 protein and mRNA is highly expressed in Term-Exh cells[79], we analyzed *CD101* mRNA transcripts from our sequencing studies and found no significant difference between WT and Gfi1^{cKO} progenitors and Ly108⁺CX$_3$CR1⁺ cells (Supplementary Fig. S5H). This further supported no formation of Term-Exh cells in the absence of Gfi1. We noted that several of the dysregulated transcripts in Gfi1^{cKO} Ly108⁺CX$_3$CR1⁺ (e.g., increased *Ikzf2 and Lef1*) that were normally downregulated in WT effector-like cells compared to progenitors (Fig. 4F and Supplementary Data File 2, 4). Overall, these data suggest that Gfi1 promotes differentiation into effector-like cells by repressing genes associated with stem-like progenitor cells.

Gfi1 is necessary for the accumulation of terminally differentiated Tim-3^{hi} CD8⁺ TILs in late-stage tumors

Our above results show that Gfi1 plays an important role in exhausted CD8⁺ T cells during chronic viral infection. Considering that tumor-infiltrating CD8⁺ T cells (TILs), like LCMV-specific CD8⁺ T cells, are also known to be exhausted due to constant antigen stimulation[3,44,80], we therefore examined whether and how Gfi1 modulates CD8⁺ TILs. First, to determine if tumor progression impacts Gfi1 expression in CD8⁺ TILs, we inoculated Gfi1tdTomato mice with MB49 tumor cells, a syngeneic model for urothelial adenocarcinoma, to establish progressive tumors (Fig. 5A). On Days 7, 14, and 22 post-tumor inoculation, CD8⁺ TILs were isolated and analyzed for TCF1 and Tim-3 expression (Fig. 5B). TCF1 mark progenitor TILs (TCF1^{hi}), and Tim-3^{hi} TILs are commonly regarded as terminally differentiated TILs[7,16]. While Day 7 CD8⁺ TILs cells were predominantly TCF1^{hi}, Tim-3^{hi} TILs emerged by Day 14 and became the dominant subset in late-stage tumors on Day 22. Day 22 Tim-3^{hi} effector cells expressed higher levels of the inhibitory receptors 2B4, LAG-3, PD-1, and TF TOX but lower levels of TF Eomes than TCF1^{hi} progenitor TILs (Fig. 5C and Supplementary Fig. S6A), while T-bet expression was comparable between the two subsets (Supplementary Fig. S6A). With respect to their Gfi1tdTomato expression, Day 7 progenitor TILs contained Gfi1tdTomato^{hi}, Gfi1tdTomato^{med}, and Gfi1tdTomato^{lo} subsets (Fig. 5D, Top). Although this pattern remained at later time points, the frequencies of Gfi1tdTomato^{lo} cells gradually decreased on Days 14-21 (Supplementary Fig. S6B), coinciding with the emergence of Tim-3^{hi} cells that were predominantly Gfi1tdTomato^{med} (Fig. 5D, Bottom & S6C). Notably, the frequencies of Gfi1tdTomato^{hi} cells were largely constant over time (Supplementary Fig. S6B). The expression of TCF1, Eomes, T-bet, and 2B4 was highest in Gfi1tdTomato^{hi} progenitor cells, whereas the expression of TOX, LAG-3, PD-1, and Tim-3 was highest in Gfi1tdTomato^{med} progenitors (Fig. 5E and Supplementary Fig. S6D). The low expression of TCF1 but high expressions of TOX, PD-1, Tim-3, and LAG-3 by Gfi1tdTomato^{med} progenitor cells mirrored that of Tim-3^{hi} cells, suggesting a close developmental interconnection between them (Fig. 5C). Altogether, these data indicate that transient downregulation of Gfi1 is a shared feature of exhausted progenitor CD8⁺ T cells during tumor progression and chronic viral infections.

To investigate the role of Gfi1 in anti-tumor responses, WT and Gfi1^{cKO} mice were inoculated with MB49 tumor cells, and tumor growth was monitored over time. While tumor growth was comparable between WT and Gfi1^{cKO} mice at the early stage, Gfi1^{cKO} mice displayed increasingly worse tumor control at later stages, corroborating our previous study in B16 melanoma[41] (Fig. 5F). Tumor mass was also greater in Gfi1^{cKO} mice on Day 21 but not on Days 7 and 12 (Fig. 5F). Frequencies of total Gfi1^{cKO} CD8⁺ T cells were increased in Day 7 tumors but decreased in Day 12 and 21 tumors compared to their WT counterparts; Gfi1^{cKO} CD8⁺ cell numbers were also significantly reduced in Day 21 tumors (Supplementary Fig. S6E–G). In contrast, the frequencies and cell numbers of total CD4⁺ TILs and FoxP3⁺ regulatory

https://doi.org/10.1038/s41467-025-59784-1

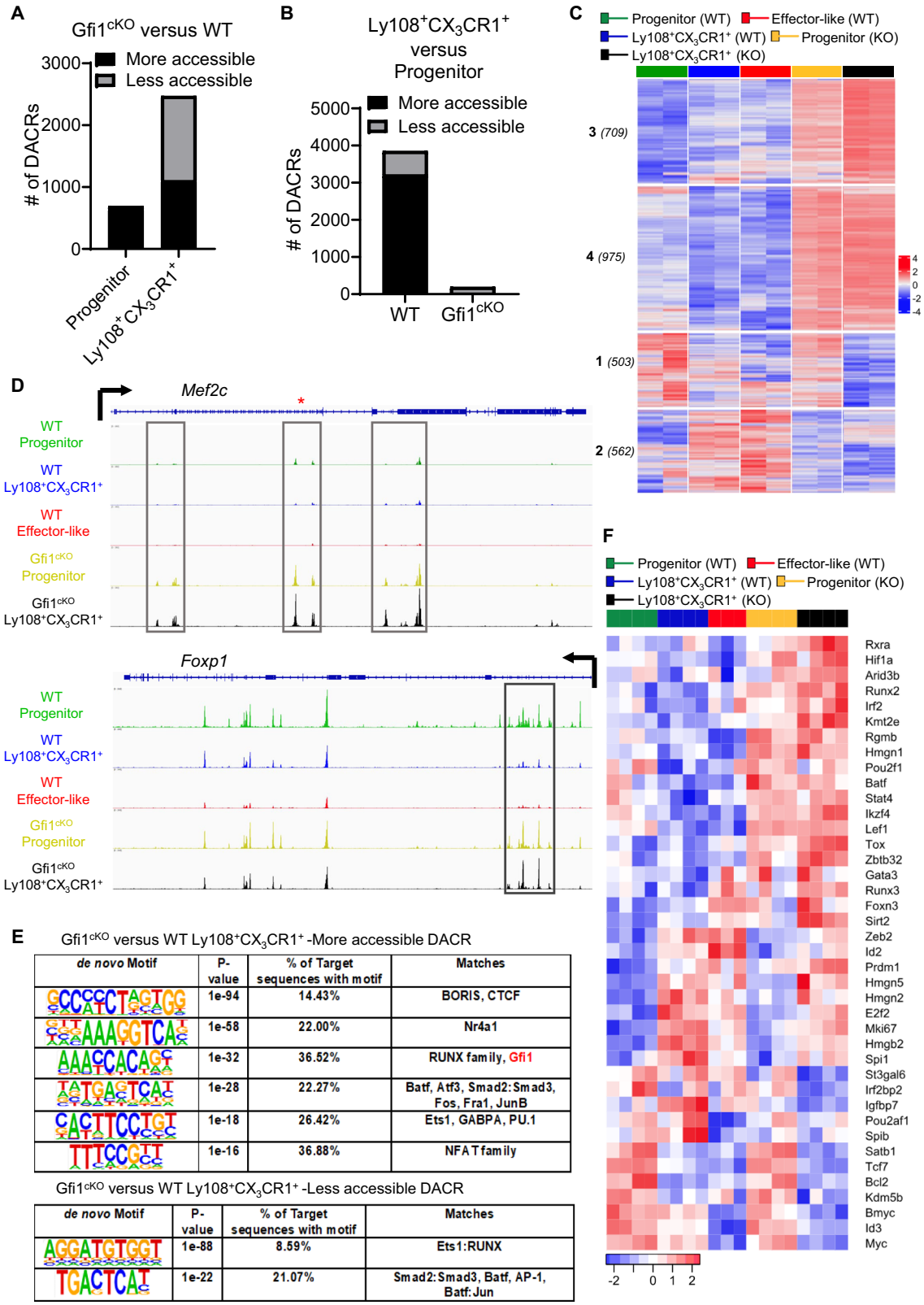

Fig. 4 | Gfi1 controls the chromatin accessibility and transcriptomic programs required for the formation of exhausted effector-like and Term-Exh CD8⁺ T cells. Exhausted GP33⁺ subsets from WT and Gfi1^{cKO} mice were sorted on Day 30 post-LCMV Cl-13 infection for ATAC-seq (**A**–**E**) or RNA-seq (**F**). **A** Differentially accessible chromatin regions (DACRs) between Gfi1^{cKO} versus WT progenitors and Ly108⁺CX$_3$CR1⁺ cells, with a cutoff of 1.2 log2 fold. **B** DACRs of progenitor versus Ly108⁺CX$_3$CR1⁺ subsets in WT and Gfi1^{cKO} cells. **C** Heatmap visualization of DACRs between Gfi1^{cKO} and WT cells were shown. *k*-means clusters with numbers of DACRs indicated in the parentheses for each cluster. **D** Genomic tracks of accessibility at *Mef2c* and *Lef1* loci in WT (progenitor, Ly108⁺CX$_3$CR1⁺, effector-like) as well as Gfi1^{cKO} (progenitors, Ly108⁺CX$_3$CR1⁺) subsets. **E** De novo HOMER motif analysis of DACRs from Gfi1^{cKO} versus WT Ly108⁺CX$_3$CR1⁺ cells. **F** Heatmap visualization of select transcripts for transcription factors in WT and Gfi1^{cKO} GP33⁺ subsets. ATAC- and RNA-seq data were from 2 and 3-4 independent replicates. Each replicate was a pooled sample of 3-5 mice.

https://doi.org/10.1038/s41467-025-59784-1

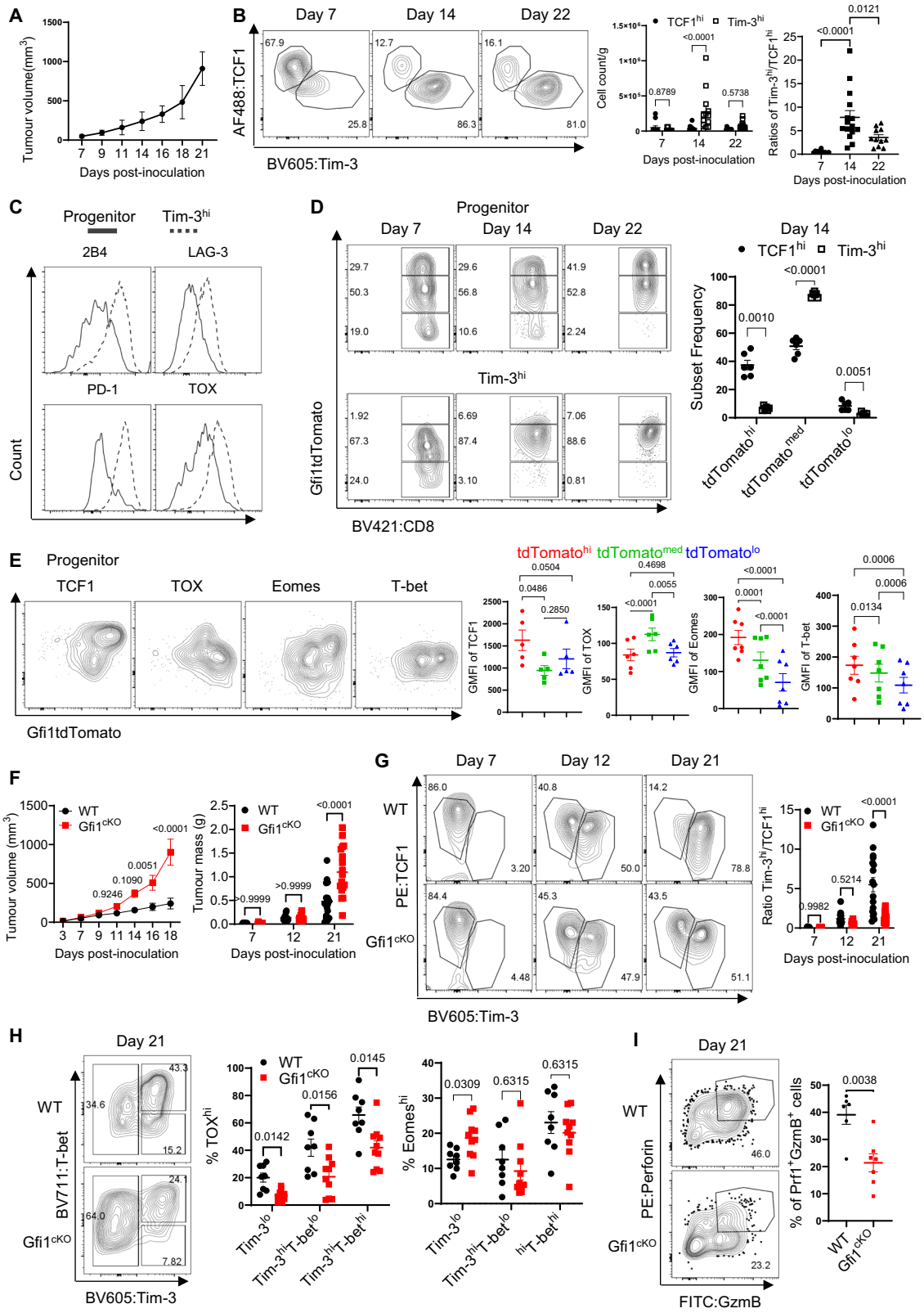

T cells (T_{reg}) were comparable between WT and Gfi1^{cKO} mice at all time points (Fig. S6E–G). In direct correlation with the reduced frequencies and numbers of CD8$^+$ TILs in late-stage tumors from Gfi1^{cKO} mice, frequencies and cell numbers of Tim-3^{hi} CD8$^+$ TILs were significantly reduced in Gfi1^{cKO} mice on Day 21 (Fig. 5G and Supplementary Fig. S6H), while the numbers of TCF1^{hi} progenitor TILs were comparable between WT and Gfi1^{cKO} mice (Supplementary Fig. S6H). Overall, these data establish a temporal requirement for Gfi1 in CD8$^+$ TILs, driving the accumulation of Tim-3^{hi} TILs at later (Day 21) but not earlier stages (Day 12) of tumor progression.

We further characterized Tim-3^{hi} TILs through examination of T-bet expression, which divided them into T-bet^{hi}Tim-3^{hi} and T-bet^{lo}Tim-3^{hi} subsets. T-bet^{hi}Tim-3^{hi} cells contained higher frequencies of TOX^{hi} cells than T-bet^{lo}Tim-3^{hi} cells, while few Tim-3^{lo} (T-

Fig. 5 | Gfi1 is necessary for the accumulation of terminally differentiated Tim-3^{hi} tumor infiltrating CD8$^+$ T cells in late-stage tumors. A Tumor growth dynamics of Gfi1tdTomato reporter mice subcutaneously inoculated with 1×10^5 MB49 cells. **B** Identification of TCF1^{hi} progenitor and Tim-3^{hi} effector CD8$^+$ TILs with total cell counts and ratios of Tim-3^{hi} to TCF1^{hi} on Days 7 ($n = 11$), 14 ($n = 13$), and 22 ($n = 11$) post-inoculation. **C** Histograms showing the expression of 2B4, LAG-3, PD-1, and TOX in TCF1^{hi} (progenitor) and Tim-3^{hi} TILs. **D** Flow plots of Gfi1tdTomato expression in progenitor and Tim-3^{hi} CD8$^+$ TILs at different time points, with the frequencies for subsets on Day 14 shown in the scatter dot plot ($n = 6$). **E** Flow plots showing expression of Gfi1tdTomato with TCF1, TOX, Eomes, and T-bet in progenitor cells with their GMFIs depicted ($n = 5$–7). **F** Tumor growth dynamics and masses on Days 7, 12, and 21 in WT ($n = 10$, 16, & 17) and Gfi1^{cKO} ($n = 11$, 16 & 18) mice post the inoculation of MB49 cells. **G** Flow plots showing the abundance of Tim-3^{hi} and TCF1^{hi} progenitor TILs in tumors from WT ($n = 10$, 18, & 17) and Gfi1^{cKO} ($n = 10$, 16, & 18) mice as well as their ratios on Day 7, 12, and 21 post-tumor inoculation. **H** Distribution of Tim-3^{hi}T-bet^{hi} and Tim-3^{hi}T-bet^{lo} effector TILs as well as Tim-3^{lo}T-bet^{int} progenitor TILs (Left) and their frequencies of TOX^{hi} and Eomes^{hi} cells (Right) on Day 21 tumors from WT ($n = 8$) and Gfi1^{cKO} ($n = 10$) mice. **I** Perforin and granzyme (**B**) production by WT ($n = 6$) and Gfi1^{cKO} ($n = 7$) CD8$^+$ TILs. Data (mean ± s.e.m.) were pooled results from 2–4 independent experiments, with each dot indicating an individual mouse. Data were analyzed by two-way ANOVA (**B** Left, **D**, **F**–**H**), one-way ANOVA (**B**, Right), repeated one-way ANOVA (**E**), and unpaired two-tail *t* test (**I**). Holm-Sidak's post hoc test was used unless otherwise stated. Source data are provided as a Source Data file.

bet^{int}) progenitor TILs were TOX^{hi} (Fig. 5H, C). Of note, T-bet^{hi}Tim-3^{hi} cells were the dominant subset in Day 21 TILs. Gfi1 deletion similarly abrogated the accumulation of both Tim-3^{hi} subsets (Supplementary Fig. S6I). The frequencies of TOX^{hi} cells were significantly reduced in both Gfi1^{cKO} progenitor and Tim-3^{hi} TILs (Fig. 5H), and Eomes^{hi} cells was only increased in Gfi1^{cKO} progenitor but not Tim-3^{hi} TILs (Fig. 5H, Right). Finally, we observed increased LAG-3 but decreased 2B4 expression in Gfi1^{cKO} Tim-3^{hi} cells, while PD-1 was comparable between WT and Gfi1^{cKO} cells (Supplementary Fig. S6I). Pan-caspase expression was similar between WT and Gfi1^{cKO} cells, excluding increased cell death as the underlying mechanism for the failed accumulation of Tim-3^{hi} cells (Supplementary Fig. S6J, Top). We did observe decreased Ki67 expression within all Gfi1^{cKO} subsets (Supplementary Fig. S6J, Bottom), consistent with a general role for Gfi1 in cell proliferation[42,81]. IFN-γ production (Supplementary Fig. S6K) and the frequency of GzmB$^+$Prf1$^+$ (Fig. 5I) cells in Gfi1^{cKO} CD8$^+$ TILs were reduced compared to WT cells. Overall, our data suggest an important role of Gfi1 in the transition of TCF1^{hi} progenitor to terminally differentiated Tim-3^{hi} TILs and their effector functions in late-stage tumors.

Gfi1 expression in T cells is required for anti-CTLA-4 efficacy

ICBs such as anti-CTLA-4/PD-1 enhance anti-tumor responses, at least in part, by promoting the proliferation of progenitor TILs and subsequent transition into terminally differentiated effector TILs[7,8,16]. Our above results indicate that transient Gfi1 downregulation in TCF1^{hi} progenitors was necessary for their transition into Tim-3^{hi} effector TILs. We therefore hypothesized that anti-CTLA-4 would induce Gfi1 downregulation in CD8$^+$ TILs. To address this, Gfi1tdTomato mice bearing MB49 tumors were treated with anti-CTLA-4 on Days 5, 8, and 11, as we previously described[82]. Anti-CTLA-4 suppressed tumor growth (Supplementary Fig. S7A), increased the infiltration of both CD4$^+$ and CD8$^+$ T cells (Supplementary Fig. S7B), and significantly reduced Gfi1tdTomato^{hi} progenitor cells (Supplementary Fig. S7C), supporting a transient Gfi1 downregulation by anti-CTLA-4. To investigate if Gfi1 in T cells mediates the therapeutic effects of anti-CTLA-4, WT and Gfi1^{cKO} mice bearing established MB49 tumors were similarly treated with anti-CTLA-4. While anti-CTLA-4 significantly inhibited tumor growth in WT mice, this did not occur in Gfi1^{cKO} mice (Fig. 6A). Similarly, anti-CTLA-4-driven infiltration and/or expansion of CD4$^+$ and CD8$^+$ TILs was observed in WT but not Gfi1^{cKO} mice (Fig. 6B). Interestingly, the increase of IFN-γ production by CD4$^+$ TILs and the reduction of T_{reg} in response to anti-CTLA-4 were comparable between WT and Gfi1^{cKO} mice (Supplementary Fig. S7D, E). Consistent with the impaired ability of Gfi1^{cKO} CD8$^+$ progenitor TILs to transition into Tim-3^{hi} TILs, Tim-3^{hi}/TCF1^{hi} ratios of CD8$^+$ TILs were significantly reduced in Gfi1^{cKO} mice compared to WT mice (Supplementary Fig. S7F), following anti-CTLA-4 treatments. Further characterizations revealed that Gfi1^{cKO} TCF1^{hi} CD8$^+$ TILs expressed higher TCF1 but lower TOX than WT cells (Supplementary Fig. S7G, H). The expression of TOX and PD-1 was comparable between WT and Gfi1^{cKO} Tim-3^{hi} subsets, although Tim-3 expression was higher in Gfi1^{cKO} Tim-3^{hi} cells (Supplementary Fig. S7H). Ki67 expression was reduced in all Gfi1^{cKO} CD8$^+$ subsets (Supplementary Fig. S7H), again supporting a general role of Gfi1 in cell proliferation[42,81]. Lastly, in contrast to no overt differences in Gfi1^{cKO} CD4$^+$ TILs, IFN-γ production was significantly reduced in Gfi1^{cKO} CD8$^+$ TILs than WT cells, upon anti-CTLA-4 therapy (Fig. 6C).

To evaluate this using another tumor model, we inoculated WT and Gfi1^{cKO} mice with MC38 cells, a widely used syngeneic model for colorectal adenocarcinoma. As in MB49 bladder tumors, anti-CTLA-4 efficacy was markedly attenuated in the Gfi1^{cKO} MC38-bearing mice compared to WT mice (Fig. 6D). Unlike the MB49 model, anti-CTLA-4 only significantly increased the infiltration of CD8$^+$ but CD4$^+$ T cells in MC38 tumors (Fig. 6E). While anti-CTLA-4-induced IFN-γ production in CD4$^+$ TIL and T_{reg} reduction were comparable between WT and Gfi1^{cKO} mice (Supplementary Fig. S7I, J), anti-CTLA-4-driven infiltration of CD8$^+$ TILs and IFN-γ production were significantly lower in Gfi1^{cKO} mice (Fig. 6F). Based on these data, we conclude that Gfi1 deletion in T cells primarily impacts CD8$^+$ TILs and renders anti-CTLA-4 therapy less effective.

Discussion

In this study, we identify 4 exhausted CD8$^+$ T cell subsets, including a previously undescribed Ly108$^+$CX$_3$CR1$^+$ population, on Day 30 post-LCMV Cl-13 infection using Ly108 and CX$_3$CR1[15] or CD44, PD-1, Ly108, TCF1, Ki67, and CD69[6]. Of note, Ly108$^+$CX$_3$CR1$^+$ cells have been gated together with effector-like cells in previous studies[6,12]. As we show here, these cells differ in phenotype, chromatin accessibility, and transcriptome from true effector-like cells. Interestingly, the expression of Gfi1, a transcriptional repressor with a previously unreported role in exhausted CD8$^+$ T cells, gradually increases and peaks on Day 30 when exhaustion is well established, following LCMV Cl-13 infection. The highest level of Gfi1 expression first emerges in precursor progenitor cells on Day 15 and remains high in exhausted progenitor, effector-like, and Term-Exh subsets but low in Ly108$^+$CX$_3$CR1$^+$ cells on Day 30. Based on these data, we propose that Gfi1 expression coincides with the emergence of exhaustion features in progenitor cells, that is propagated to effector-like and Term-Exh cells, in line with the model proposed by Utzschneider et al.[9]. Gfi1 loss in CD8$^+$ T cells blocks the formation of effector-like and Term-Exh subsets, whereas the generation of progenitors and Ly108$^+$CX$_3$CR1$^+$ cells is unaffected. As a result, viral titers are higher in Gfi1^{cKO} mice at later time points. Considering the phenotype of Gfi1^{cKO} CD8$^+$ T cells on Day 15 post-LCMV Cl-13 infection and the previously proposed replacement of short-lived effector cells at this time point[9], we hypothesize that Ly108$^+$CX$_3$CR1$^+$ cells likely emerge ~2 weeks post-infection, although we were unable to isolate these cells to test this hypothesis, due to their continually changing phenotype during the first 3-4 weeks after infection[9,15].

Adoptive transfer of exhausted subsets reveals divergent developmental potential of these cells. While effector-like and Term-Exh cells retain their phenotype and progenitors expectedly repopulate all the other subsets, Ly108$^+$CX$_3$CR1$^+$ cells only develop into effector-like and Term-Exh cells but not progenitors. Interestingly, our data indicate

https://doi.org/10.1038/s41467-025-59784-1

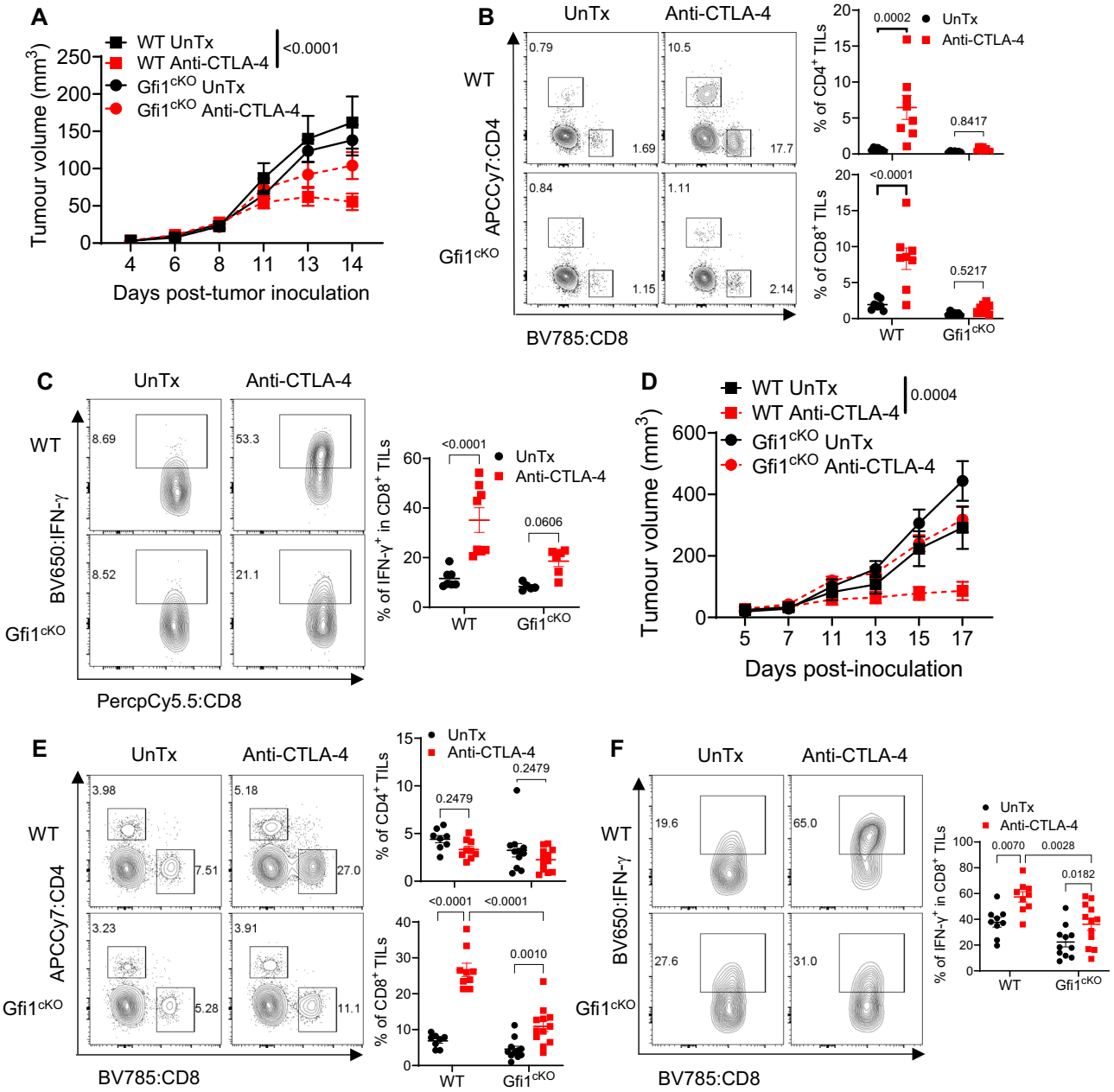

Fig. 6 | Gfi1 expression in T cells is required for anti-CTLA-4 efficacy. WT and Gfi1^{cKO} mice inoculated with MB49 cells were treated with anti-CTLA-4 on Days 5, 8, and 11 post-inoculation. Tumor growth dynamics was depicted in the line graph (**A**, $n = 4$). Tumors were harvested to evaluate the infiltration of CD4$^+$ and CD8$^+$ T cells (**B**, $n = 7$ for untreated and 8 for treated groups of both WT and Gfi1^{cKO} mice) and IFN-γ production by CD8$^+$ TILs (**C**, $n = 7$ for untreated WT mice, = 8 for treated WT mice, = 5 for untreated Gfi1^{cKO} mice, and = 6 for treated Gfi1^{cKO} mice). **D** WT ($n = 4$ in the untreated group and = 5 in the treated group) and Gfi1^{cKO} ($n = 7$ in the untreated group and 5 in the treated group) mice bearing palpable MC38 bladder tumors were treated with or without anti-CTLA-4 on Days 5, 8, and 11 post-tumor inoculation. Tumor growth dynamics was shown in the line graph. **E**, **F** Tumors were harvested to evaluate the infiltration of CD4$^+$ and CD8$^+$ T cells (**E** $n = 8$ for untreated WT and 9 for treated WT; $n = 11$ for untreated Gfi1^{cKO} and 12 for treated Gfi1^{cKO}) and IFN-γ production by CD8$^+$ TILs (**F** $n = 9$ for untreated and treated WT; $n = 11$ for untreated Gfi1^{cKO} and 12 for treated Gfi1^{cKO}). Data (mean ± s.e.m.) were pooled results from 2-3 independent experiments, with each dot denoting a mouse. Two-way ANOVA with Holm-Sidak post hoc test was used. Source data are provided as a Source Data file.

that Ly108$^+$CX$_3$CR1$^+$ cells also retain their identify for some time, suggesting some degree of their stability. Previous studies assessing the heterogeneity of the effector-like cells have identified KLRG-expressing intermediate precursor cells[12–14]. Putting our findings in that context, we argue that Ly108$^+$CX$_3$CR1$^+$ cells are an even earlier intermediate precursor population to effector-like and Term-Exh cells. Collectively, these results support earlier studies showing a bifurcation in the development of effector-like and Term-Exh cells[12–14], a decision likely made at the Ly108$^+$CX$_3$CR1$^+$ and not stem-like progenitor state. While results from the viral infection studies with Gfi1^{cKO} mice indicate Gfi1 expression is needed for the differentiation of Ly108$^+$CX$_3$CR1$^+$ cells into effector-like or Term-Exh cells, it nevertheless does not commit a particular fate. Future work should focus on factors dictating fate decisions, which likely involve CD4$^+$ T cell help[15].

Systemic comparisons of Gfi1tdTomato^{lo} and Gfi1tdTomato^{hi} fractions in the progenitor, effector-like, and Term-Exh subsets suggest repression of TOX, Eomes, and Tim-3 by Gfi1. In further support, we observe increased expressions of TOX and Tim-3 in both Gfi1^{cKO}

progenitors and Ly108$^+$CX$_3$CR1$^+$ compared to their WT counterparts, while an increase in Eomes was only observed in Gfi1^{cKO} progenitors, likely due to its already high expression in WT Ly108$^+$CX$_3$CR1$^+$ cells. Complex transcriptomic and epigenetic imprinting govern subset diversification. In the absence of Gfi1, progenitor and Ly108$^+$CX$_3$CR1$^+$ cells exhibit increased accessibility at the *Mef2c* locus, which is normally lost in WT effector-like and Term-Exh cells, suggesting Gfi1 may promote the formation of effector-like cells by suppressing accessibility at this locus. Consistent with this, the *Mef2c* transcript is significantly higher in Ly108$^+$CX$_3$CR1$^+$ than effector-like cells. Our RNA-seq analysis also identify a repressive role for Gfi1 in the expression of other genes such as *Lef1, Hmgn1, Stat4*, and *Ikzf2*. These genes are typically associated with the progenitor population but downregulated in effector-like or Term-Exh cells. These results, together with the adoptive transfer data and functional studies, suggest that Gfi1 represses genes associated with the stem-like progenitor cells, thereby facilitating the formation of effector-like and Term-Exh cells.

We notice considerable differences among exhausted CD8$^+$ T cells from chronic viral infections versus tumors, which reflect the distinction between systemic versus local antigen distribution, different cellular niches, and the rather harsh tumor microenvironment. Despite this, we show that Gfi1 is similarly expressed at a high level in a subset of TCF1^{hi} progenitor TILs. Transient downregulation of Gfi1 in the progenitor TILs precedes the emergence of terminally differentiated effector Tim-3^{hi} cells, similar to the Gfi1 downregulation in Ly108$^+$CX$_3$CR1$^+$ prior to the formation of effector-like and Term-Exh cells during chronic viral infections. Moreover, deletion of Gfi1 impairs the accumulation of Tim-3^{hi} TILs in late-stage tumors. Interestingly, Gfi1 is seemingly dispensable for the generation of Tim-3^{hi} effector TILs during the early stage of tumor development, suggesting a temporal requirement of Gfi1. To this end, a previous study report that CD8$^+$ TILs undergo distinct chromatin states in late-stage tumors when they become refractory to ICBs[83]. Our results suggest the switch of the reprogrammability in CD8$^+$ TILs might be partially mediated by Gfi1, warranting future investigations. Of note, both Gfi1^{cKO} progenitor CD8$^+$ T cells from chronic viral infection and tumors exhibit increased Eomes as well as LAG-3 expression. Despite the reported role of LAG-3 in sustaining TOX expression in both tumors and chronic viral infections[84,85], we observe increased TOX expression in Gfi1^{cKO} cells from the chronic viral infection but decreased TOX expression in Gfi1^{cKO} CD8$^+$ TILs, suggesting additional regulatory mechanisms controlling TOX expression in chronic infections versus cancer. Although we are unable to directly determine Gfi1 binding sites in this study, due to technical challenges and limited cell numbers, these results warrant future studies examining Gfi1 binding sites and its interactions with TOX, other TFs (e.g., Eomes), and inhibitory receptors such as LAG-3.

T cell exhaustion is a major barrier to immunotherapies (e.g., CAR-T and ICBs)[4,8,86,87]. Our study identifies an important role of Gfi1 in orchestrating CD8$^+$ T cell response to anti-CTLA-4 therapy, the very first FDA-approved ICB to treat patients with advanced cancer[88]. We reason that fine-tuning Gfi1 activity in T cells may prevent or reverse T cell exhaustion to bolster ICB efficacy. Considering Gfi1 downregulation is associated with the active differentiation of progenitors, we argue that transient and intermittent inhibition of Gfi1 with lysine specific histone demethylase (LSD1)[33] may facilitate the differentiation of progenitors to Ly108$^+$CX$_3$CR1$^+$ cells and then to effector-like cells, thereby improving the control of chronic infections and tumors, as a standalone therapy or in combination with ICBs. To this end, a recent study reports promising outcomes from combining an LSD1 inhibitor (Bomedemstat) with anti-PD-1 in small cell lung cancer[89]. Further testing of this combination approach should be conducted in melanoma, bladder cancer, and colorectal adenocarcinoma, especially those resistant to ICBs[90]. Elucidating the aforementioned interactions of Gfi1 with its binding partners (e.g., CoREST, NuRD, or CtBP complexes[35], Eomes, LAG-3, and others yet to be defined) during CD8$^+$ T cell responses will be beneficial in devising rational therapeutic strategies to combat cancer and chronic infections.

Methods

Mice

Gfi1tdTomato mice were generated by Dr. Lacaud[45] and transferred to us from Dr. Grimes, with permission from Dr. Lacaud. Gfi1$^{fl/fl}$ mice, as we previously described[36,41], were generated by Dr. Hano Hock[38] and provided to us by Dr. Hongbo Chi, in agreement with Dr. Hock. They were bred with transgenic CD4-Cre mice as heterozygotes at the CD4-Cre locus (Gfi1^{cKO}) and littermates (CD4-Cre$^{-/-}$) (WT). Male and female mice were used in all experiments, unless specified. B6.SJL-Ptprca-Pepcb/BoyJ mice (CD45.1$^+$) were obtained from the Jackson Laboratory. CD45.1 mice were crossed with Gfi1$^{fl/fl}$CD4-Cre$^{-/-}$ (WT) mice to generate CD45.1$^+$CD45.2$^+$ mice, which were used as recipients in the bone marrow chimera studies. C57BL/6J-*Ptprcem6Lutzy*/J mice (JAX-Boy, CD45.1$^+$) were a gift from Dr. Zajac and used in the adoptive transfer experiments. All mice were bred and maintained in a specific pathogen-free animal facility at The University of Alabama at Birmingham (UAB), under a 12 h/12 h light/dark cycle, ambient room temperature (22 °C), and 40– 70% humidity. 7– 12 weeks old mice were used in the experiments, and protocols were approved by the Institutional Animal Care and Use Committee at UAB.

LCMV Infection, bone marrow chimeras, and adoptive transfer of LCMV$^+$ CD8$^+$ cells

For LCMV infections, 4×10^6 plaque-forming-units (PFU) of LCMV Cl-13 (chronic infection) were intravenously injected into Gfi1^{cKO} and littermate control (WT) mice via the tail vein. 2×10^5 PFU of LCMV Armstrong were injected intraperitoneally. At designated times post-infection, sera were collected and frozen until used in the plaque assay to determine viral titers using Vero cells. In brief, Vero cells were cultured in 6-well plates to confluency. Culture media was removed, and 200 µL of diluted sera was added to the plates for 1 h at 37 °C. Cells were then overlayed with a mixture of 1% agarose and medium 199 (Sigma-Aldrich) and cultured for 4 days at 37 °C. Cells were overlayed again with a 1:1 mixture of 1% agarose and medium 199 supplemented with 0.02% of neutral red solution (Sigma-Aldrich). Cells were incubated at 37 °C overnight before plaques were enumerated under a light source.

To generate the mixed bone marrow chimeras, recipient CD45.1$^+$CD45.2$^+$ mice were lethally irradiated with 2 doses of 500 Rad with an at least 4-hour interval in between and reconstituted with 1×10^7 bone marrow cells depleted of mature T cells from CD45.1$^+$ mice and CD45.2$^+$ Gfi1$^{fl/fl}$CD4-Cre$^{-/-}$ (littermate controls, WT) or Gfi1$^{fl/fl}$CD4-Cre$^{+/-}$ (Gfi1^{cKO}) mixed at 1:1 ratio. After > 6 weeks of reconstitution, mice were similarly infected with LCMV Cl-13. In the CD4$^+$ T cell depletion experiments, in vivo neutralizing antibodies against CD4 (Bio X Cell, clone GK1.5, #BE0003-1) (300 µg/mouse) were injected intraperitoneally 1 day before and 3 days after LCMV infection.

For adoptive cell transfer, freshly prepared splenocytes from Day 30 LCMV Cl-13 infected Gfi1tdTomato reporter mice were sorted for GP33$^+$ subsets (Ly108$^+$CX$_3$CR1$^-$ progenitors, Ly108$^+$CX$_3$CR1$^+$ cells, Ly108$^-$CX$_3$CR1$^+$ effector-like cells, and Ly108$^-$CX$_3$CR1$^-$ Term-Exh cells,) or Gfi1tdTomato^{hi} versus Gfi1tdTomato^{lo} progenitors using BD FACSAria SORP-Titan. Sorted cells were adoptively transferred into CD45.1 JAX-boy mice (~ 8×10^4 subset cells or (~ 2×10^4 Gfi1tdTomato$^{hi/lo}$ progenitors cells per mouse), and mice were infected with 4×10^6 PFU LCMV Cl-13 on the next day. Spleens from recipient mice were harvested on Day 8 post-infection for fate-mapping of adoptively transferred cells.

In vivo tumor inoculation and treatment

The chemically induced murine urothelial adenocarcinoma MB49 cells and colorectal adenocarcinoma MC38 cells, kindly provided by Dr. Ashish Kamat and Dr. Jim Allison at MD Anderson Cancer Center, was originally derived from a male and a female C57BL/6 mouse,

respectively. These cells were cultured in Dulbecco's modified Eagle's medium with 10% fetal bovine serum (FBS) at 37 °C, 5% CO_2, with regular testing for mycoplasma using the MycoAlert detection kit (Lonza, LT07-118) to ensure they were free of mycoplasma contamination. For tumor inoculation, exponentially growing MB49 cells (1×10^5) and MC38 cells (5×10^5) with a passage number less than 10 were subcutaneously injected into the shaved right flanks of male and female mice, respectively. On D5 post-tumor inoculation, mice received anti-CTLA-4 or isotype antibodies intraperitoneally (i.p.), with the first dose at 200 μg/mouse and subsequent doses of 100 μg/mouse on D8 and 11. Tumor measurements were taken 2–3 times/week, starting from D3 post-tumor inoculation. Following our IACUC protocols, mice were euthanized when tumors reached 2.0 cm in diameter, developed ulceration, or the mice became moribund.

TIL isolation and tissue preparation

Detailed procedures were described previously[41,91]. In brief, tumors were collected in ice-cold RPMI 1640 containing 2% FBS and minced into fine pieces, followed by digestion with 400 μ/mL collagenase D (Worthington Biochemical Corporation, #LS004186) and 20 μg/mL DNase I (Sigma, #10104159001) at 37 °C for 40 min with periodic shaking. EDTA (Sigma, #1233508) was then added at a final concentration of 10 mM to stop digestion. Cell suspensions were filtered through 70 μM cell strainers, and TILs were obtained by collecting the cells in the interphase after Ficoll (MP Biomedicals, #091692254) gradient separation. Spleens and livers were collected in ice-cold HBSS containing 2% FBS. Single cell suspensions from spleens were generated through disruption on a wire screen (infection studies) or nylon nano mesh (tumor studies); Red blood cells were lysed with 0.84% (w/v) NH_4Cl or ACK lysis buffer (Thermo Scientific). Livers were minced and digested with Collagenase IV and DNase I in Hank's balanced salt solution for 30 mins at 37 °C. Digested tissue was separated after centrifugation over Ficoll (MP Biomedicals, #091692254) and washed with complete media. Cells were resuspended in RPMI 1640 medium supplemented with 50 μM β-mercaptoethanol, penicillin (100 μ/ml), streptomycin (100 mg/ml), and either 1 or 10% fetal bovine serum (FBS) or Click's media (Irvine Scientific, #9195-500 mL) containing 10% FBS, 10% Pen/Strep, and 10% Glutamine for flow cytometric analyses, as described below.

Flow cytometric analyses

Flow cytometry data were collected on a BD FACSymphony with BD FACSDiva software or an Invitrogen AttuneNXT cytometer with Attune cytometric software. All data were analyzed with FloJo. Live-Dead staining was done using the aqua fluorescent reactive dye (ThermoFisher Scientific, L34966A) prior to surface staining. For surface and tetramer staining, cells were stained for 30– 40 mins at 4 °C. For transcription factor staining, cells were fixed and permeabilized with the eBioscience Foxp3/Transcription Factor staining kit (ThermoFisher Scientific, 00-5523-00) before staining with antibodies for 30–45 mins at 4 °C. To measure intracellular cytokines, for the LCMV studies, freshly prepared splenocytes from Day 30 LCMV Cl-13 infected mice were stimulated with GP33 peptides in the presence of monensin (BD Biosciences, #51-2092KZ) for 4 h prior to surface staining and intracellular cytokine detection using the BD CytoFix/Cytoperm buffer kit. (BD, 554714). For tumor studies, freshly isolated TILs were stimulated ex vivo with PMA/Ionomycin in the presence of monensin (BD Biosciences, #51-2092KZ) for 4 h prior to surface staining and intracellular cytokine detection. Antibodies used for flow cytometry included: anti-mouse 2B4 (m2B4 (B6) 458.1, Biolegend, 1:200), anti-mouse Ly108 (330-AJ, Biolegend, 1:200), anti-mouse Tim-3 (RMT3-23, Biolegend, 1:200), anti-mouse/human CD44 (IM7, Biolegend, 1:200), anti-mouse CD8a (53-6.7. BD, 1:200), anti-mouse CD8a (53-6.7, Invitrogen, 1:200), mouse anti-TCF7/TCF1 (S33-966, BD, 1:100), anti-mouse CX_3CR1 (SA011F11, Biolegend, 1:200), anti-PD-1 (RMP1-30, BD, 1:150), anti-KLRG1 (2F1, Invitrogen, 1:200), anti-CXCR6 (SA051D1, Biolegend, 1:200), anti-mouse CD45.1 (A20, Biolegend, 1:200), anti-mouse CD45.2 (104, Biolegend, 1:200), anti-mouse CD4 (RM4-5, Biolegend, 1:200), anti-mouse/Rat FoxP3 (FJK-16s, Invitrogen, 1:100), anti-mouse TCRβ (H57-597, Biolegend, 1:200), anti-IFN-γ (XMG1.2, Biolegend, 1:100), anti-TNF (MP6-XT22, Biolegend, 1:100), anti-mouse CD101 (mousehi101, eBioscience, 1:200), anti-mouse CD69 (H1.2F3, BD, 1:200), anti-mouse LAG-3 (C9B7W, Biolegend, 1:200), anti-mouse Ki67 (11F6, Biolegend, 1:100), anti-mouse Eomes (Dan11mag, Invitrogen, 1:100), anti-human/mouse TOX (REA473, Miltenyi, 1:100), anti-mouse T-bet (4B10, Biolegend, 1:100), anti-mouse Perforin (S16009A, Biolegend, 1:100), anti-human/mouse Granzyme B (QA16A02, Biolegend, 1:100). H2-DbGP33 (1:200) tetramers were acquired from the National Institutes of Health (NIH) Tetramer Core at Emory University.

Bulk RNA-seq

Freshly prepared splenocytes from Day 30 LCMV CL-13 infected mice were sorted for bulk populations of $GP33^+$ subsets using the BD FACSAria SORP Titan. Three to five mice were pooled for each replicate. Cells were homogenized in TRIzol LS reagent (Invitrogen, 10296028) and total RNA was isolated. Library preparation, quality control, and paired-end sequencing was performed at GeneWiz Inc. RNA-seq data analysis was done as we previously described[91]. In brief, sequences were adapter and quality trimmed with Trim Galore (v0.6.10) and aligned to the mm10 reference genome[92] using Star (v2.7.11a)[93]. Counts were generated with HTSeq (v2.0.5)[94]. Differential analysis using glmTreat was performed using edgeR (v3.42.4)[95], and heatmaps were generated using limma (v 3.56.2)[96].

Assay for transposase-accessible chromatin with sequencing (ATAC-seq)

ATAC-seq libraries for bulk-sorted populations, as described above, were generated using a previously published protocol[97]. Library quality control and paired end PE150 sequencing was performed by Novogene Co. For data analysis, reads were adapter and quality trimmed using Trim Galore (v 0.6.10). Trimmed fastq files were aligned to the mm10 reference genome[92] with Bowtie2 (v2.4.3) using the following settings bowtie2 -p 10 --very-sensitive -k 10 -X 2000. Genrich (v0.6.1) was used to define peaks from biological replicates using the following settings –j –r -s 10 -v. Regions aligned to the mitochondrial chromosome and the Encode defined blacklist regions[98] were excluded during peak calling with Genrich. Bedgraphs from Genrich were used to generate bigwig files using the UCSC utility bedGraphToBigWig. Narrowpeak files for all samples were merged using BEDTools (v2.28), converted to the SAF format, and counts were generated using featureCounts (v.2.0.6)[99]. Differential analysis using glmTreat with lfc ≥ 1.2 or glmQLFTest was performed using edgeR (v3.42.4)[95], and heatmaps were generated using limma (v 3.56.2)[96] and ComplexHeatmap[100]. Genomic range objects were generated using GenomicRanges (v1.52.1) and annotated with ChipSeeker (v1.36.0)[101]. Pathway enrichment analysis was performed using ClusterProfiler (v4.8.3)[102]. Venn diagrams were generated with ggVennDiagram (v.15.0)[103]. HOMER (v4.11)[65] was used for motif analysis. Genomic tracks were viewed and generated with Integrative Genomics Viewer (v2.16.1)[104].

Statistical analysis

All experiments were repeated 2–5 times. Results were depicted as mean ± s.e.m. Data were analyzed using a two-sided Student's *t* test, one-way ANOVA, or two-way ANOVA after confirming their normal distribution. All analyses were performed using Prism 10.2.0

(GraphPad Software, Inc.), and $p < 0.05$ was considered statistically significant.

Reporting summary

Further information on research design is available in the Nature Portfolio Reporting Summary linked to this article.

Data availability

The bulk RNA-seq and ATAC-seq data have been deposited in the Gene Expression Omnibus (GEO) database under accession codes: GSE261250. All sequencing data have been made publicly available. Source data are provided in this paper.

Code availability

The codes for analyzing RNA-seq and ATAC-seq data deposited in the GEO database (GSE261250) are publicly available[105].

References

1. Blank, C. U. et al. Defining 'T cell exhaustion. *Nat. Rev. Immunol.* **19**, 665–674 (2019).
2. Zajac, A. J. et al. Viral immune evasion due to persistence of activated T cells without effector function. *J. Exp. Med.* **188**, 2205–2213 (1998).
3. Mueller, S. N. & Ahmed, R. High antigen levels are the cause of T cell exhaustion during chronic viral infection. *Proc. Natl. Acad. Sci. USA* **106**, 8623–8628 (2009).
4. Utzschneider, D. T. et al. T Cell factor 1-expressing memory-like CD8(+) T cells sustain the immune response to chronic viral infections. *Immunity* **45**, 415–427 (2016).
5. Bucks, C. M., Norton, J. A., Boesteanu, A. C., Mueller, Y. M. & Katsikis, P. D. Chronic antigen stimulation alone is sufficient to drive CD8+ T cell exhaustion. *J. Immunol.* **182**, 6697–6708 (2009).
6. Beltra, J. C. et al. Developmental relationships of four exhausted CD8(+) T cell subsets reveals underlying transcriptional and epigenetic landscape control mechanisms. *Immunity* **52**, 825–841 (2020).
7. Siddiqui, I. et al. Intratumoral Tcf1(+)PD-1(+)CD8(+) T cells with stem-like properties promote tumor control in response to vaccination and checkpoint blockade immunotherapy. *Immunity* **50**, 195–211 (2019).
8. Im, S. J. et al. Defining CD8+ T cells that provide the proliferative burst after PD-1 therapy. *Nature* **537**, 417–421 (2016).
9. Utzschneider, D. T. et al. Early precursor T cells establish and propagate T cell exhaustion in chronic infection. *Nat. Immunol.* **21**, 1256–1266 (2020).
10. Chen, Z. et al. TCF-1-Centered transcriptional network drives an effector versus exhausted CD8 T cell-fate decision. *Immunity* **51**, 840–855 (2019).
11. Paley, M. A. et al. Progenitor and terminal subsets of CD8+ T cells cooperate to contain chronic viral infection. *Science* **338**, 1220–1225 (2012).
12. Kasmani, M. Y. et al. Clonal lineage tracing reveals mechanisms skewing CD8+ T cell fate decisions in chronic infection. *J. Exp. Med.* **220**, https://doi.org/10.1084/jem.20220679 (2023).
13. Daniel, B. et al. Divergent clonal differentiation trajectories of T cell exhaustion. *Nat. Immunol.* **23**, 1614–1627 (2022).
14. Giles, J. R. et al. Shared and distinct biological circuits in effector, memory and exhausted CD8(+) T cells revealed by temporal single-cell transcriptomics and epigenetics. *Nat. Immunol.* **23**, 1600–1613 (2022).
15. Zander, R. et al. CD4(+) T Cell help is required for the formation of a cytolytic CD8(+) T cell subset that protects against chronic infection and cancer. *Immunity* **51**, 1028–1042 (2019).
16. Miller, B. C. et al. Subsets of exhausted CD8(+) T cells differentially mediate tumor control and respond to checkpoint blockade. *Nat. Immunol.* **20**, 326–336 (2019).
17. Tsui, C. et al. MYB orchestrates T cell exhaustion and response to checkpoint inhibition. *Nature* **609**, 354–360 (2022).
18. Chen, Y. et al. BATF regulates progenitor to cytolytic effector CD8(+) T cell transition during chronic viral infection. *Nat. Immunol.* **22**, 996–1007 (2021).
19. Yao, C. et al. BACH2 enforces the transcriptional and epigenetic programs of stem-like CD8(+) T cells. *Nat. Immunol.* (2021).
20. Baxter, A. E. et al. The SWI/SNF chromatin remodeling complexes BAF and PBAF differentially regulate epigenetic transitions in exhausted CD8(+) T cells. *Immunity* **56**, 1320–1340 (2023).
21. Kharel, A. et al. Loss of PBAF promotes expansion and effector differentiation of CD8(+) T cells during chronic viral infection and cancer. *Cell Rep.* **42**, 112649 (2023).
22. Khan, O. et al. TOX transcriptionally and epigenetically programs CD8(+) T cell exhaustion. *Nature* **571**, 211–218 (2019).
23. Scott, A. C. et al. TOX is a critical regulator of tumour-specific T cell differentiation. *Nature* **571**, 270–274 (2019).
24. Seo, H. et al. TOX and TOX2 transcription factors cooperate with NR4A transcription factors to impose CD8(+) T cell exhaustion. *Proc. Natl. Acad. Sci. USA* **116**, 12410–12415 (2019).
25. Yao, C. et al. Single-cell RNA-seq reveals TOX as a key regulator of CD8(+) T cell persistence in chronic infection. *Nat. Immunol.* **20**, 890–901 (2019).
26. McDonald, B. et al. Canonical BAF complex activity shapes the enhancer landscape that licenses CD8(+) T cell effector and memory fates. *Immunity* **56**, 1303–1319 (2023).
27. Lin, Y. et al. The SNAG domain of Snail1 functions as a molecular hook for recruiting lysine-specific demethylase 1. *EMBO J.* **29**, 1803–1816 (2010).
28. Zweidler-Mckay, P. A., Grimes, H. L., Flubacher, M. M. & Tsichlis, P. N. Gfi-1 encodes a nuclear zinc finger protein that binds DNA and functions as a transcriptional repressor. *Mol. Cell Biol.* **16**, 4024–4034 (1996).
29. Anguita, E., Villegas, A., Iborra, F. & Hernandez, A. GFI1B controls its own expression binding to multiple sites. *Haematologica* **95**, 36–46 (2010).
30. Fiolka, VassenL., Mahlmann, K. & Moroy, S. T. Direct transcriptional repression of the genes encoding the zinc-finger proteins Gfi1b and Gfi1 by Gfi1b. *Nucleic Acids Res.* **33**, 987–998 (2005).
31. Shi, L. Z. & Chi, H. Gfi1: A unique controller of Treg cells. *Cell Cycle* **12**, 3581–3582 (2013).
32. Doan, L. L. et al. Targeted transcriptional repression of Gfi1 by GFI1 and GFI1B in lymphoid cells. *Nucleic Acids Res.* **32**, 2508–2519 (2004).
33. Saleque, S., Kim, J., Rooke, H. M. & Orkin, S. H. Epigenetic regulation of hematopoietic differentiation by Gfi-1 and Gfi-1b is mediated by the cofactors CoREST and LSD1. *Mol. Cell* **27**, 562–572 (2007).
34. McClellan, D. et al. Growth factor independence 1B-mediated transcriptional repression and lineage allocation require lysine-specific demethylase 1-dependent recruitment of the BHC complex. *Mol. Cell Biol.* **39**, https://doi.org/10.1128/mcb.00020-19 (2019).
35. Helness, A. et al. GFI1 tethers the NuRD complex to open and transcriptionally active chromatin in myeloid progenitors. *Commun. Biol.* **4**, 1356 (2021).
36. Shi, L. Z. et al. Gfi1-Foxo1 axis controls the fidelity of effector gene expression and developmental maturation of thymocytes. *Proc. Natl. Acad. Sci. USA* **114**, E67–E74 (2017).
37. Yucel, R., Karsunky, H., Klein-Hitpass, L. & Moroy, T. The transcriptional repressor Gfi1 affects development of early,

uncommitted c-Kit+ T cell progenitors and CD4/CD8 lineage decision in the thymus. *J. Exp. Med.* **197**, 831–844 (2003).
38. Hock, H. et al. Intrinsic requirement for zinc finger transcription factor Gfi-1 in neutrophil differentiation. *Immunity* **18**, 109–120 (2003).
39. Schmidt, T. et al. Evidence implicating Gfi-1 and Pim-1 in pre-T-cell differentiation steps associated with beta-selection. *EMBO J.* **17**, 5349–5359 (1998).
40. Schmidt, T. et al. Zinc finger protein GFI-1 has low oncogenic potential but cooperates strongly with pim and myc genes in T-cell lymphomagenesis. *Oncogene* **17**, 2661–2667 (1998).
41. Shi, L. Z. et al. Inhibitory role of the transcription repressor Gfi1 in the generation of thymus-derived regulatory T cells. *Proc. Natl. Acad. Sci. USA* **110**, E3198–E3205 (2013).
42. Karsunky, H., Mende, I., Schmidt, T. & Moroy, T. High levels of the onco-protein Gfi-1 accelerate T-cell proliferation and inhibit activation induced T-cell death in Jurkat T-cells. *Oncogene* **21**, 1571–1579 (2002).
43. Yucel, R., Kosan, C., Heyd, F. & Moroy, T. Gfi1:green fluorescent protein knock-in mutant reveals differential expression and autoregulation of the growth factor independence 1 (Gfi1) gene during lymphocyte development. *J. Biol. Chem.* **279**, 40906–40917 (2004).
44. Schietinger, A. et al. Tumor-Specific T Cell Dysfunction Is a Dynamic Antigen-Driven Differentiation Program Initiated Early during Tumorigenesis. *Immunity* **45**, 389–401 (2016).
45. Thambyrajah, R. et al. GFI1 proteins orchestrate the emergence of haematopoietic stem cells through recruitment of LSD1. *Nat. Cell Biol.* **18**, 21–32 (2016).
46. Gerlach, C. et al. The chemokine receptor CX3CR1 defines three antigen-experienced CD8 T cell subsets with distinct roles in immune surveillance and homeostasis. *Immunity* **45**, 1270–1284 (2016).
47. Wherry, E. J., Blattman, J. N., Murali-Krishna, K., van der Most, R. & Ahmed, R. Viral persistence alters CD8 T-cell immunodominance and tissue distribution and results in distinct stages of functional impairment. *J. Virol.* **77**, 4911–4927 (2003).
48. Blackburn, S. D., Shin, H., Freeman, G. J. & Wherry, E. J. Selective expansion of a subset of exhausted CD8 T cells by alphaPD-L1 blockade. *Proc. Natl. Acad. Sci. USA* **105**, 15016–15021 (2008).
49. Tsao, H. W. et al. Batf-mediated epigenetic control of effector CD8(+) T cell differentiation. *Sci. Immunol.* **7**, eabi4919 (2022).
50. Grusdat, M. et al. IRF4 and BATF are critical for CD8(+) T-cell function following infection with LCMV. *Cell Death Differ.* **21**, 1050–1060 (2014).
51. Yao, C. et al. BACH2 enforces the transcriptional and epigenetic programs of stem-like CD8(+) T cells. *Nat. Immunol.* **22**, 370–380 (2021).
52. Hnisz, D. et al. Super-enhancers in the control of cell identity and disease. *Cell* **155**, 934–947 (2013).
53. Saoudi, A., Kassem, S., Dejean, A. and Gaud, G. Rho-GTPases as key regulators of T lymphocyte biology. *Small GTPases* **5**, https://doi.org/10.4161/sgtp.28208 (2014).
54. Gattinoni, L. et al. Wnt signaling arrests effector T cell differentiation and generates CD8+ memory stem cells. *Nat. Med.* **15**, 808–813 (2009).
55. McCutcheon, S. R. et al. Transcriptional and epigenetic regulators of human CD8(+) T cell function identified through orthogonal CRISPR screens. *Nat. Genet.* **55**, 2211–2223 (2023).
56. Doedens, A. L. et al. Hypoxia-inducible factors enhance the effector responses of CD8(+) T cells to persistent antigen. *Nat. Immunol.* **14**, 1173–1182 (2013).
57. Man, K. et al. Transcription factor IRF4 promotes CD8(+) T cell exhaustion and limits the development of memory-like T cells during chronic infection. *Immunity* **47**, 1129–1141 (2017).
58. Yan, J., Pandey, S. P., Barnes, B. J., Turner, J. R. & Abraham, C. T Cell-intrinsic IRF5 regulates T cell signaling, migration, and differentiation and promotes intestinal inflammation. *Cell Rep.* **31**, 107820 (2020).
59. Ben Nasr, M. et al. Glucagon-like peptide 1 receptor is a T cell-negative costimulatory molecule. *Cell Metab.* **36**, 1302–1319 (2024).
60. Wong, C. K. et al. Divergent roles for the gut intraepithelial lymphocyte GLP-1R in control of metabolism, microbiota, and T cell-induced inflammation. *Cell Metab.* **34**, 1514–1531 (2022).
61. Wang, D. et al. The transcription factor Runx3 establishes chromatin accessibility of cis-regulatory landscapes that drive memory cytotoxic T lymphocyte formation. *Immunity* **48**, 659–674 (2018).
62. Milner, J. J. et al. Runx3 programs CD8(+) T cell residency in non-lymphoid tissues and tumours. *Nature* **552**, 253–257 (2017).
63. Shan, Q. et al. The transcription factor Runx3 guards cytotoxic CD8(+) effector T cells against deviation towards follicular helper T cell lineage. *Nat. Immunol.* **18**, 931–939 (2017).
64. Cruz-Guilloty, F. et al. Runx3 and T-box proteins cooperate to establish the transcriptional program of effector CTLs. *J. Exp. Med.* **206**, 51–59 (2009).
65. Heinz, S. et al. Simple combinations of lineage-determining transcription factors prime cis-regulatory elements required for macrophage and B cell identities. *Mol. Cell* **38**, 576–589 (2010).
66. Kurachi, M. et al. The transcription factor BATF operates as an essential differentiation checkpoint in early effector CD8+ T cells. *Nat. Immunol.* **15**, 373–383 (2014).
67. Martinez, G. J. et al. The transcription factor NFAT promotes exhaustion of activated $CD8^+$ T cells. *Immunity* **42**, 265–278 (2015).
68. Harberts, A. et al. Interferon regulatory factor 4 controls effector functions of CD8(+) memory T cells. *Proc. Natl. Acad. Sci. USA* **118**, https://doi.org/10.1073/pnas.2014553118 (2021).
69. Yao, S. et al. Interferon regulatory factor 4 sustains CD8(+) T cell expansion and effector differentiation. *Immunity* **39**, 833–845 (2013).
70. Miyagawa, F. et al. Interferon regulatory factor 8 integrates T-cell receptor and cytokine-signaling pathways and drives effector differentiation of CD8 T cells. *Proc. Natl Acad. Sci. USA* **109**, 12123–12128 (2012).
71. Moroy, T. The zinc finger transcription factor Growth factor independence 1 (Gfi1). *Int J. Biochem. Cell Biol.* **37**, 541–546 (2005).
72. Grimes, H. L., Chan, T. O., Zweidler-McKay, P. A., Tong, B. & Tsichlis, P. N. The Gfi-1 proto-oncoprotein contains a novel transcriptional repressor domain, SNAG, and inhibits G1 arrest induced by interleukin-2 withdrawal. *Mol. Cell Biol.* **16**, 6263–6272 (1996).
73. Zander, R. et al. Tfh-cell-derived interleukin 21 sustains effector CD8(+) T cell responses during chronic viral infection. *Immunity* **55**, 475–493 (2022).
74. McLane, L. M. et al. Role of nuclear localization in the regulation and function of T-bet and Eomes in exhausted CD8 T cells. *Cell Rep.* **35**, 109120 (2021).
75. Ghoneim, H. E. et al. De novo epigenetic programs inhibit PD-1 blockade-mediated T cell rejuvenation. *Cell* **170**, 142–157 (2017).
76. Chalmin, F. et al. Stat3 and Gfi-1 transcription factors control Th17 cell immunosuppressive activity via the regulation of ectonucleotidase expression. *Immunity* **36**, 362–373 (2012).
77. Shan, Q. et al. Tcf1-CTCF cooperativity shapes genomic architecture to promote CD8(+) T cell homeostasis. *Nat. Immunol.* **23**, 1222–1235 (2022).
78. Martinez, G. J. et al. The transcription factor NFAT promotes exhaustion of activated CD8(+) T cells. *Immunity* **42**, 265–278 (2015).
79. Hudson, W. H. et al. Proliferating transitory T cells with an effector-like transcriptional signature emerge from PD-1(+) stem-like CD8(+) T cells during chronic infection. *Immunity* **51**, 1043–1058 (2019).

80. Blattman, J. N., Wherry, E. J., Ha, S. J., van der Most, R. G. & Ahmed, R. Impact of epitope escape on PD-1 expression and CD8 T-cell exhaustion during chronic infection. *J. Virol.* **83**, 4386–4394 (2009).
81. Zhu, J. et al. Growth factor independent-1 induced by IL-4 regulates Th2 cell proliferation. *Immunity* **16**, 733–744 (2002).
82. Shi, L. Z. et al. Interdependent IL-7 and IFN-gamma signalling in T-cell controls tumour eradication by combined alpha-CTLA-4+alpha-PD-1 therapy. *Nat. Commun.* **7**, 12335 (2016).
83. Philip, M. et al. Chromatin states define tumour-specific T cell dysfunction and reprogramming. *Nature* **545**, 452–456 (2017).
84. Ngiow, S. F. et al. LAG-3 sustains TOX expression and regulates the CD94/NKG2-Qa-1b axis to govern exhausted CD8 T cell NK receptor expression and cytotoxicity. *Cell* **187**, 4336–4354 (2024).
85. Andrews, L. P. et al. LAG-3 and PD-1 synergize on CD8(+) T cells to drive T cell exhaustion and hinder autocrine IFN-gamma-dependent anti-tumor immunity. *Cell* **187**, 4355–4372 (2024).
86. Long, A. H. et al. 4-1BB costimulation ameliorates T cell exhaustion induced by tonic signaling of chimeric antigen receptors. *Nat. Med.* **21**, 581–590 (2015).
87. Wu, T. et al. The TCF1-Bcl6 axis counteracts type I interferon to repress exhaustion and maintain T cell stemness. *Sci. Immunol.* **1**, https://doi.org/10.1126/sciimmunol.aai8593 (2016).
88. Leach, D. R., Krummel, M. F. & Allison, J. P. Enhancement of antitumor immunity by CTLA-4 blockade. *Science* **271**, 1734–1736 (1996).
89. Hiatt, J. B. et al. Inhibition of LSD1 with bomedemstat sensitizes small cell lung cancer to immune checkpoint blockade and T-cell killing. *Clin. Cancer Res.* **28**, 4551–4564 (2022).
90. Gao, J. et al. Loss of IFN-gamma pathway genes in tumor cells as a mechanism of resistance to anti-CTLA-4 therapy. *Cell* **167**, 397–404 (2016).
91. Shen, H. et al. Selective suppression of melanoma lacking IFN-γ pathway by JAK inhibition depends on T cells and host TNF signaling. *Nat. Commun.* **13**, 5013 (2022).
92. Mouse Genome Sequencing, C. et al. Initial sequencing and comparative analysis of the mouse genome. *Nature* **420**, 520–562 (2002).
93. Dobin, A. et al. STAR: ultrafast universal RNA-seq aligner. *Bioinformatics* **29**, 15–21 (2013).
94. Putri, G. H., Anders, S., Pyl, P. T., Pimanda, J. E. & Zanini, F. Analysing high-throughput sequencing data in Python with HTSeq 2.0. *Bioinformatics* **38**, 2943–2945 (2022).
95. Robinson, M. D., McCarthy, D. J. & Smyth, G. K. edgeR: a Bioconductor package for differential expression analysis of digital gene expression data. *Bioinformatics* **26**, 139–140 (2010).
96. Ritchie, M. E. et al. limma powers differential expression analyses for RNA-sequencing and microarray studies. *Nucleic Acids Res.* **43**, e47 (2015).
97. Grandi, F. C., Modi, H., Kampman, L. & Corces, M. R. Chromatin accessibility profiling by ATAC-seq. *Nat. Protoc.* **17**, 1518–1552 (2022).
98. Amemiya, H. M., Kundaje, A. & Boyle, A. P. The ENCODE Blacklist: Identification of problematic regions of the genome. *Sci. Rep.* **9**, 9354 (2019).
99. Liao, Y., Smyth, G. K. & Shi, W. featureCounts: an efficient general purpose program for assigning sequence reads to genomic features. *Bioinformatics* **30**, 923–930 (2014).
100. Gu, Z. Complex heatmap visualization. *Imeta* **1**, e43 (2022).
101. Wang, Q. et al. Exploring epigenomic datasets by ChIPseeker. *Curr. Protoc.* **2**, e585 (2022).
102. Wu, T. et al. clusterProfiler 4.0: A universal enrichment tool for interpreting omics data. *Innovation* **2**, 100141 (2021).
103. Gao, C. H., Yu, G. & Cai, P. ggVennDiagram: An intuitive, easy-to-use, and highly customizable R package to generate venn diagram. *Front. Genet.* **12**, 706907 (2021).
104. Robinson, J. T. et al. Integrative genomics viewer. *Nat. Biotechnol.* **29**, 24–26 (2011).
105. Ojo, O. A. et al. Gfi1 controls the formation of effector-like CD8+ T cells during chronic viral infections and cancer. *Nat. Comms.* https://doi.org/10.1038/s41467-025-59784-1 (2025). In Press

Acknowledgements

We thank other members of the Shi lab and the research team in the Department of Radiation Oncology for their constructive input. We thank Dr. Leighton Grimes from Cincinnati Children's Hospital for transferring the Gfi1tdTomato mice to us, and Brittany Curtiss & Sajesan Aryal from Dr. Rui Lu Lab (UAB) for the protocol of sample preparation and data analysis for ATAC-Seq. We thank Dr. Chris Willey for his help during the paper revision. We are grateful for Haley Kvarnberg's help with the viral titer assays. We would also like to thank Sagar Hanumanthu and other members of the UAB flow cytometry and single cell facility for sorting cells. We are grateful for the Startup fund from the Department of Radiation Oncology and the O'Neal Invests pre-R01 Grant from the UAB-O'Neal Comprehensive Cancer Center to L.Z.S. This study is partially funded by National Institutes of Health grants (1R21CA230475-01A1, 1R21CA259721-01A1, and 1R01CA279849-01A1 to L.Z.S., and 5R01AI156290 to A.J.Z.), the V Foundation Scholar Award (V2018-023 to L.Z.S.), a DoD-Congressionally Directed Medical Research Programs grant (ME210108 to L.Z.S.), a Cancer Research Institute CLIP Grant (CRI4342) to L.Z.S., and an American Cancer Society Institutional Research Grant (91-022-19) to L.Z.S.

Author contributions

O.A.O. designed and performed experiments with mice and cells, analyzed data, and contributed to writing the manuscript. H.S. and J.T.I. did experiments with mice and cells. J.A.B., R.S.W., and A.J.Z. contributed to manuscript construction, data analyses, discussion, and manuscript editing. A.J.Z. provided LCMV viral stocks and working space. L.G. established and provided the Gfi1tdTomato reporter mice. L.Z.S. was responsible for the original conceptualization of this study, overall data presentation, and manuscript construction; L.Z.S. acquired most of the funding for this study, designed experiments, supervised laboratory studies and data analyses, wrote and edited the manuscript. All authors have met the requirements for authorship and agree to the content in this publication.

Competing interests

The authors declare no competing interests.

Additional information

Supplementary information The online version contains supplementary material available at https://doi.org/10.1038/s41467-025-59784-1.

Correspondence and requests for materials should be addressed to Lewis Z. Shi.

Peer review information *Nature Communications* thanks Grégory Verdeil and the other anonymous reviewers for their contribution to the peer review of this work. A peer review file is available.